# The biophysical basis of protein domain compatibility in ion channels

Willow Coyote-Maestas[1], David Nedrud[1], Antonio Suma[2], Yungui He[3], Kenneth A. Matreyek[4], Douglas M. Fowler[5,6], Vincenzo Carnevale[2], Chad L. Myers[7], Daniel Schmidt[3]

[1]Department of Biochemistry, Molecular Biology & Biophysics, University of Minnesota, Minneapolis, MN, 55455, USA

[2] Department of Chemistry, Temple University, Philadelphia, PA, 19122, USA

[3] Department of Genetics, Cell Biology & Development, University of Minnesota, Minneapolis, MN, 55455, USA

[4] Department of Pathology, Case Western Reserve University School of Medicine, Cleveland, OH, 44106, USA

[5] Department of Genome Sciences, University of Washington, Seattle, WA, 98115, USA

[6] Department of Bioengineering, University of Washington, Seattle, WA, 98115, USA

[7] Department of Computer Science and Engineering, University of Minnesota, Minneapolis, MN, 55455, USA

**Summary:**

Massively parallel assays reveal interactions between donor domains and recipient proteins govern domain compatibility

**Abstract:**

Understanding the biophysical mechanisms that govern the combination of protein domains into viable proteins is essential for advancing synthetic biology and biomedical engineering. Here, we use massively-parallel genotype/phenotype assays to determine cell surface expression of over 300,000 variants of the inward rectifier $K^+$ channel Kir2.1 recombined with hundreds of protein motifs. We use machine learning to derive a quantitative biophysical model and practical rules for domain recombination. Insertional fitness depends on nonlinear interactions between the biophysical properties of inserted motifs and the recipient protein, which adds a new dimension to the rational design of fusion proteins. Insertion maps reveal a generalizable hierarchical organization of Kir2.1 and several other ion channels that balances stability needed for folding and dynamics required for function.

34 **Main text:**

35 Protein domains are basic evolutionary units that allow the rapid emergence of new
36 proteins by domain recombination (*1*). Accordingly, domain recombination-based
37 approaches are often used to generate synthetic proteins in biomedical engineering (*2*).
38 However, synthetically recombined proteins that fold and function well are typically the
39 result of trial-and-error and iterative optimization. Furthermore, deriving practical rules
40 that accelerate domain recombination-based protein design is challenging because
41 structure/function relationships of isolated and recombined domains differ (*3*).

42

43 To derive rules for productive domain recombination, we generated 760 polypeptide motif
44 (donor) insertions at all 436 amino acids of the inward rectifier $K^+$ channel Kir2.1
45 (recipient) and then measured cell surface expression of the resulting channel/insertion
46 variants. Previously, we found surprising variability between three motif's insertional
47 profiles, which implies donor-recipient compatibility being complex (*4*). We chose 760
48 donor motifs as a representative sample to exhaustively study compatibility (**Supp. Table**
49 **1**). The massive scale of these experiments (over 300,000 variants) is possible due to
50 insertional libraries with little bias (*5*) (**Supp. Fig. 1**) and recombining libraries into stable
51 cell lines (*6*).

52

53 ***Systematic motif insertions reveal strong fitness pattern consistent with known ion***
54 ***channel biochemistry***

55 Kir2.1 helps maintain cellular excitability (*7*). For Kir2.1 to function it must fold,
56 tetramerize, and traffic to the plasma membrane (*8–12*). We measure the impact of
57 insertions on Kir2.1 with fluorescent antibody labeling and fluorescently activated cell
58 sorting coupled to sequencing (**Fig. 1A**). To quantify how motif insertions affect Kir2.1
59 surface expression, we calculate surface expression fitness of insertion variants as
60 enrichment or depletion of surface expressed vs. non-surface expressed variants. This
61 data is consistent with expected biochemistry (**Fig. 1B-C**). Insertions into the extracellular
62 FLAG tag, used to label surface-expressed Kir2.1, decrease trafficking fitness because
63 they disrupt antibody binding. Motif insertions into transmembrane regions (M1, M2, Pore,

64 Filter) strongly decrease fitness (Wilcoxon rank sum test p-value < 2.2e-16) presumably
65 by impairing membrane insertion of the nascent protein (*8*, *13*). Similarly, insertions in
66 folding-critical core beta sheets of the C-terminal domain (CTD) (*14*) decrease fitness.
67 Conversely, most insertions in the unstructured N- or C-termini are tolerated. As
68 expected, insertions into Golgi export signals decrease surface expression. This is
69 particularly strong for a N-terminal signal with tertiary structure (**Fig. 1B**, positions 46-50,
70 (*11*)). On the other hand, insertion phenotypes in an ER export signal (the unstructured
71 FCYENE signal (*9*), **Fig. 1B**, positions 382-387) are more varied with some not affecting
72 surface trafficking. Perhaps the specific residue orientation that is required for function in
73 structured export signal renders them more sensitive to motif insertion, while linear
74 unstructured signals that rely on localized charge or hydrophobicity are more robust.
75 Although insertional fitness patterns are overall consistent with known biochemistry, the
76 variability of insertion fitness across donor motifs and recipient insertion implies more
77 complex mechanisms for domain compatibility.
78
79 ***Recipient and donor properties interact to determine insertion fitness***
80 To learn if donor properties affect fitness, we hierarchically clustered insertion fitness by
81 motif. This revealed three groups: short unstructured motifs, larger folded motifs, and
82 hydrophobic motifs (**Fig. 1B**). Unstructured motifs are allowed in many parts of Kir2.1.
83 Structured motifs, which contain nearly all motifs longer than 90 amino acids, are most
84 allowed at the termini and spuriously in structured Kir2.1 regions. Hydrophobic motifs are
85 distinct from other motifs clusters. They decrease fitness in regions (e.g., N terminus) that
86 are universally compatible with the other two motif groups. Some hydrophobic motifs can
87 be inserted where no other motifs can (e.g. beginning of M1 and end of M2
88 transmembrane helices). Taken together, this suggests that insertion fitness is influenced
89 by the inserted motif's properties.
90
91 To learn if recipient protein properties affect fitness, we used Uniform Manifold
92 Approximation and Projection (UMAP (*15*)) clustering by insertion position. Three distinct
93 clusters emerge (**Supp. Fig. 2A**) corresponding to contiguous regions of Kir2.1 (**Fig. 1D**).

These regions represent the (1) pore domain and CTD core beta sheets, (2) unstructured N- and C-termini, and (3) $PIP_2$ (Kir2.1's activator) binding sites, interfaces between the pore domain / CTD, and monomer interfaces within CTD. The emergence of discrete contiguous Kir2.1 regions from unbiased clustering suggests that local Kir2.1 properties influence insertional fitness, as well.

To identify the underlying biophysical properties that influence insertion fitness, we calculated sequence-, structure-, and dynamics-based properties of inserted motifs (**Supp. Table 2**) and recipient Kir2.1 (**Supp. Table 3**). We find that insertion fitness has moderately positive correlation with Kir2.1 backbone flexibility (molecular dynamics-derived root mean square fluctuation and anisotropic network model-derived stiffness; Pearson correlation coefficient 0.48 and -0.41, respectively, **Fig. 2A**) implying that Kir2.1 rearranges structurally after motif insertion. Available space at insertion sites (e.g., contact degree) has a non-monotonic relationship (**Fig. 2B**). Inserted motif clusters have distinct property distributions. This implies that the pattern of insertion fitness correlates with the biophysical properties of the motif. (**Fig. 2C-H**). This is illustrated by a subcluster comprised of longer motifs containing hydrophobic and negatively charged residues (black box in **Fig 1B, Fig. 2F-H**). While motif properties are clearly important, they behave non-linearly. For example, correlation of insertion fitness with motif length is negative for motifs under 25 amino acids, but becomes positive for longer motifs (-0.33 and 0.22 Pearson coefficients, respectively, **Fig. 2I**). Remarkably, all motif properties correlate positively and negatively with fitness dependent on insertion position. Motif lengths, for example, is positively correlated in flexible termini and loops but negatively correlated in the G-loop (**Fig. 2M**). Our data provide highly-resolved information about both donor motifs and the recipient channel that captures the specific rules that govern insertional compatibility (**Fig. 2M, Supp. Fig. 3**). Hierarchical clustering correlations between fitness and motif properties at each residue separates Kir2.1 into three distinct classes (**Fig. 2L, Supp. Fig. 4**). These classes are similar to UMAP clustering of fitness alone (compare **Fig. 1D** and **Fig. 2L**, Pearson's $\chi 2$ test p-value $< 2.2e-16$, Cramer's V 0.42), which indicates that motif and recipient properties can explain insertion fitness. Within each

124 class, correlation sign (positive or negative) between fitness with inserted donor
125 properties is identical. For example, all residues in the pore domain and beta sheet core
126 of the CTD class positively correlate with motif hydrophobicity and negatively with polarity
127 (**Supp. Fig. 4**). Overall, this suggests that biophysical properties underlie insertional
128 compatibility and properties of Kir2.1 (recipient) and inserted motif (donor) interact to
129 determine fitness.
130
131 ***Machine learning reveals the basis for donor/recipient compatibility***
132 To identify which donor and recipient properties are important and how they interact in
133 compatible insertions, we used Machine Learning (ML). While ML methods are
134 sometimes treated as black boxes, they are useful for exploring rich genotype/phenotype
135 datasets with non-linear interactions (*16*). We trained and tested regression random
136 forests to predict insertional fitness at every amino acid position based on recipient and
137 motif properties. To identify the most important properties and aid interpretation, we
138 reduced properties from over 900 to 10 based on redundancy and feature importance
139 with little impact on performance (**Supp. Fig. 5, Supp. Table 4**). The final model
140 successfully predicts insertional fitness for all positions and motifs of data withheld from
141 model training (**Supp. Fig. 6**).
142
143 Local Kir2.1 flexibility (RMSF and stiffness) is important for model performance and is
144 positively associated with insertion fitness (**Fig. 3A,E, Supp. Fig. 7C,G**). Insertion
145 position space (contact degree) plays a major non-linear role (**Fig. 3A,E**). Apart from
146 contact degree, all recipient properties have simple monotonic relationships with
147 insertional fitness meaning recipient properties determine whether an insertion is viable
148 (**Supp. Fig. 7**).
149
150 The most important motif properties are length and hydrophobicity, which are both
151 bimodal (**Fig. 3C-D**). To understand why length and hydrophobicity are bimodal and how
152 properties interact, we explored all property interactions **(Fig. 3F-G)**. While recipient
153 properties do not interact with each other, we find motif properties do interact amongst

154 themselves and with recipient properties **(Fig. 3G)**. This suggests motif property
155 interactions determine insertion fitness and not all insertions are equally compatible with
156 each insertion position.
157
158 By exploring property interactions, we learn why different motifs behave distinctly (**Supp.**
159 **Note 1, Supp. Figs. 8-10**). For example, low contact degree is strongly beneficial for
160 large motifs (**Supp. Fig. 8H**). Highly hydrophobic short donor motifs are deleterious within
161 flexible regions (small flexible loops) likely because their solvent-exposed hydrophobic
162 residues will be destabilizing and promote aggregation (**Fig. 3H-I**) (*17*). The small motif
163 cluster contains motifs that are shorter and less hydrophobic, which makes them less
164 disruptive (**Fig. 2C-D, Supp. Fig. 9B-C**). In contrast, highly hydrophobic motifs are best
165 allowed in buried regions with high stiffness and contact degree because these insertion
166 positions minimize solvent exposure (**Fig. 3H-I, Supp. Fig. 10G**). Longer motifs benefit
167 from strong positive interactions between motif length and moderate hydrophobicity likely
168 allowing the formation of a hydrophobic core that can promote folding (**Fig. 3J, Supp.**
169 **Fig. 8D**) (*18*). Well-folded domains can be stabilizing and promote insertion fitness when
170 there is sufficient space otherwise large insertions disrupt the recipient protein's folding
171 (**Supp. Fig. 8H**). Formation of a stable hydrophobic core as a desirable property of
172 engineered domains corroborates conclusions from high-throughput protein design
173 experiments (*19*).
174
175 The ML model allows us to propose practical rules for successfully inserting donor motifs
176 into recipient proteins. Insertion positions are ideally located in flexible protein regions
177 with sufficient space. To form a well-folded domain, motifs need sufficient length and
178 hydrophobic amino acid content to form a well-ordered hydrophobic core. If a desired
179 insertion position is located within a buried and rigid region an inserted motif should be
180 hydrophobic. More flexible regions prefer small non-hydrophobic insertions, and larger
181 more structured domains will only be allowed if there is sufficient space and flexibility.
182 Most significantly, the interactions between motifs and recipient properties determine the

183 outcome of protein recombination. This adds a new dimension to other domain
184 recombination approaches that implicitly treat donor motifs as interchangeable (*20*).
185
186 Motif and recipient property interactions produce the distinct classes of motifs and regions
187 (**Fig. 1B,D, Fig. 2L**). The rigid class with TM and CTD core beta sheets requires specific
188 conformations to achieve a stable fold and allows few insertions. The flexible class with
189 the N/C termini can adopt many conformations and allows most insertions. The class
190 representing interfaces is an intermediate that is structured and dynamic. It contains many
191 Kir2.1 regions ($PIP_2$ binding site, TM/CTD and subunit interfaces) that conformationally
192 change upon $PIP_2$ binding and during closed to open state transitions (*21*, *22*). Since
193 gating mechanisms are conserved across the inward rectifier family (*23*), the interface
194 class may also be enriched for other inward rectifier regulator binding sites, such as $G\beta\gamma$
195 (GIRK), and ATP (Kir6.2). This is indeed the case (p-value < 2e-16, two-sided Fisher's
196 Exact test, **Supp. Fig. 14**). Taken together, classes suggest a hierarchical organization
197 of inward rectifiers that balance the stability needed for folding with the conformational
198 dynamics required for function.
199
200 ***A hierarchical organization of ion channels that balances stability and flexibility for***
201 ***folding and function***
202 To test if our compatibility framework and the hierarchical organization generalizes, we
203 profiled surface expression fitness in the inward rectifier Kir3.1 (GIRK), the voltage-
204 dependent $K^+$ channels Kv1.3, the purinoreceptor $P2X_3$, and the acid-sensing channel
205 Asic1a by inserting a smaller set of 15 motifs (**Fig. 4A**, **Supp. Table 5, Supp. Fig. 11**).
206 Kir3.1 is a G-protein regulated paralog of Kir2.1 with very similar structure (*23*) but
207 requires co-expression of Kir3.2 for effective trafficking (*10*). Kv1.3, $P2X_3$, and Asic1a
208 have different folds, gating, and regulation (*24–26*).
209
210 The general patterns of surface expression in inward rectifiers also apply to Kv1.3, $P2X_3$,
211 and Asic1a. There is weak to moderate correlation between the relative impact of each
212 domain (**Supp. Fig. 12-13**) in different channels, suggesting that while inserted motifs

213 have similar effects across channels, the recipient channel's properties dominate. For
214 related channels –Kir2.1 and Kir3.1– insertion profiles are fairly correlated (Pearson
215 correlation coefficient 0.56). Insertions in membrane-embedded regions are deleterious,
216 insertions into termini are allowed, and different inserted motifs give rise to distinct fitness
217 profiles (**Supp. Fig. 11**). This suggests that properties that dictate fitness in Kir2.1 are
218 generalizable to other ion channels.
219 Since properties manifested as distinct classes in Kir2.1, we wondered if this concept
220 would also apply to Kir3.1, Kv1.3 and P2X3. Applying the same UMAP-based clustering
221 approach we used for Kir2.1, we find discrete insertion fitness classes in all channels
222 (**Fig. 4B**). As expected from shared fold architecture, Kir3.1's classes resemble Kir2.1's
223 (Pearson's $\chi 2$ test p-value <2.2e-16, Cramer's V 0.36) with three classes encompassing
224 the TM and CTD core, regulator binding sites and interfaces, and termini. Using
225 established structure/function data, we can infer that classes have distinct roles in folding
226 stability and conformational dynamics. In each channel, there is a class that allows few
227 insertions and corresponds to structural element required for tetramerization (Kv1.3 T1
228 tetramerization domain), folding (inward rectifier CTD Ig-like fold (14), $P2X_3$ disulfide-
229 stabilized ecto-domain (28), and Asic1a beta sheets), or membrane insertion
230 (transmembrane helices). Most channels have a class that allows nearly all insertions,
231 and which coincides with flexible protein termini. The final class is intermediate, allowing
232 only certain insertions. The intermediate class is enriched for residues that
233 conformationally change during gating or regulation (e.g., Kir TM/CTD interface (*21*),
234 Kv1.3 S1-T1 linker (*29*), $P2X_3$ cytoplasmic cap (*25*)).
235 We propose class organization is a universal feature of ion channels that results from
236 constraints on channel structure to satisfy folding, assembly, and interaction with
237 trafficking partners while providing flexibility for allosteric regulation and conformational
238 changes during channel opening and closing. Other studies proposed a similar protein
239 'sector' concept, based on analyzing coevolution of residue pairs in large alignments
240 across homologues (*30*). In contrast, our classes emerge from direct experimental data
241 that are not constrained by statistical modeling's limitations and reflect underlying
242 biophysical properties. Insertional profiling could be useful as a high-throughput coarse-

243 grain structural biology method to study protein folding and dynamics from steady-state
244 biochemical experiments. Further experiments are required to establish whether the
245 hierarchical organization of insertion fitness extends to all protein classes.
246
247 Our dataset provides an unprecedented depth of information across hundreds of inserted
248 donor motifs and several recipient ion channels. Using this dataset, we build a quantitative
249 biophysical model of domain recombination in ion channels. Our discovery of specific
250 interactions between donor and recipient properties is a crucial step towards universal
251 domain recombination 'grammar' (*31*) for rational engineering of fusion proteins.
252 Unbiased clustering of insertion fitness reveals a hierarchical organization of ion channels
253 into regions with different material properties (rigid, semi-flexible, flexible) that play distinct
254 roles to balance the stability needed for trafficking and the dynamics required for gating.
255 As a universal organizing framework, this may explain how contradictory requirements
256 for stability and flexibility can be balanced to allow for well-folded and functional proteins.
257
258 **Contributions**
259 W.C.-M., D.S., and D.N. conceived the study. W.C.-M. and D.N. generated libraries and
260 performed insertional scans. D.N. coded alignment and enrichment pipelines for data
261 analysis. W.C.-M. carried out machine learning, correlation analysis, and data mining.
262 D.S. conducted clustering analysis and structural mapping. A.S. and V.C. conducted
263 molecular dynamics simulations. K.A.M. and D.M.F. provided reagents and technical
264 advice to construct mammalian cell lines from libraries. C.L.M. provided expertise for
265 random forest model building and data mining. W.C.-M. and D.S. co-wrote the manuscript
266 with input from all co-authors.
267
268 **Acknowledgements**
269 We thank James Fraser, Gabriella Estevam, Margaret Titus, the Schmidt Lab, and Fraser
270 lab for helpful feedback and discussion. We acknowledge support from the University of
271 Minnesota Flow Cytometry Resource, in particular Rashi Arora, Therese Martin, and
272 Jason Motl for providing flow cytometry technical support. Andrei Lupas and Vikram Alva

kindly provided motif sequences from previous studies. Hellen Farrants and Kai Johnsson kindly provided DHFR and cpDHFR DNA for experiments.

**Funding**

This work was supported by the National Institutes of Health [MH109038 to D.S.] and a University of Minnesota Genome Center Illumina S2 grant. W.C.-M. is supported by a National Science Foundation Graduate Research Fellowship and a Howard Hughes Medical Institute Gilliam Fellowship for Advanced Study.

## Figure Legends

**Figure 1: Large-scale insertional fitness profiling.** (**A**) Motifs are inserted into all positions of a recipient protein using SPINE (*5*). A stable single-copy insertion library is generated by BxBI-mediated recombination in HEK293T (*6*). Cells are sorted based on channel surface expression determined by antibody labelling of an extracellular FLAG tag. Genotypes of each sorted cell population are recovered by NGS. (**B**) Insertion fitness heatmap of 760 motifs inserted into all positions of Kir2.1. Secondary structural elements (grey boxes) are Kir2.1 are shown above, along known Golgi and ER export signals (green and magenta boxes, respectively). Motifs are hierarchically clustered using a cosine distance metric. Dendrograms are colored by major motifs groups. The black box indicates a subset of 'well-structured motifs' (see Fig. 2F-H). **(C-D**) Mean normalized insertion fitness (**C**) or UMAP classification of Kir2.1 insertion fitness (**D**) mapped onto the structure of Kir2.2 (PDB: 3SPI (*21*); 70% identity with Kir2.1; residues 1-40 and 379-410 are modelled). Fitness classes describe conformationally rigid and structured pore domain and CTD beta sheet core (class 1; cyan), highly flexible and unstructured N/C termini (class 2; red), and structured yet dynamic interface between TM and CTD, or between subunit in the CTD (class 3; yellow). $PIP_2$ (Kir2.1's activator) is show in magenta.

**Figure 2: Relationships between fitness data and computed properties.** Pairwise scatterplots between recipient properties (**A** – RMSF, **B** – contact degree**)** and insertion fitness. (**C-E**) Boxplots of motif (**C**) length, (**D**) hydrophobicity, and (**E**) negativity across

303 the three motif clusters from Fig. 1B. Median is marked with a block line, boxes represent
304 the interquartile range, outlier points are shown, and p values from a pairwise Wilcoxon
305 tests are shown. (**F-H**) Density plots of motif (**F**) length, (**G**) hydrophobicity, and (**H**)
306 negativity of the domain cluster and all other motifs colored. Density is weighted group
307 size to allow direct comparison between different sized groups. (**I-K**) Pairwise scatterplots
308 between motif properties (**I** – motif length and **J** – NC termini distance, **K** – motif
309 hydrophobicity) and insertion fitness. (**L**) Hierarchical clusters of motif properties
310 correlations with Kir2.1 position (Supp. Fig. 3) is mapped onto the structure of Kir2.2
311 (PDB: 3SPI (*21*); 70% identity with Kir2.1; residues 1-40 and 379-410 are modelled). The
312 regulator $PIP_2$ is shown in magenta. (**M**) Spearman correlation plot between motif
313 properties and the fitness of that motif at each position. Properties are hierarchically
314 clustered. A LOESS regression curve is fitted to each scatterplot, with the red line
315 represents the fit and the gray area represents the 95% confidence interval. Boxplot
316 significance levels are *** $p<0.001$, ** $p<0.01$, and * $p<0.05$, respectively.
317
318 **Figure 3: Machine learning model.** (**A**) Bar plots of recipient or donor property
319 importance in predicting insertion fitness. Importance is based on the mean absolute error
320 of removing features from the predictive model. (**B-E**) Plots of the Accumulated local
321 effects (ALE) of properties on prediction insertion fitness for (**B**) recipient contact degree,
322 (**C**) motif hydrophobicity, (**D**) motif length, and (**E**) recipient RMSF. (**F, G**) Heatmap of
323 each property's interaction strength overall (**F**) and pairwise (**G**) with every other property.
324 (**H-J**) Pairwise ALE plots investigate how pairwise interactions contribute to prediction of
325 (**H**) recipient stiffness-motif hydrophobicity, (**I**) recipient stiffness-motif length, and (**J**)
326 motif hydrophobicity-motif length. Pairwise ALE plots are colored from dark blue to pink
327 with increasing ALE scores. Marginal ticks (**B-E, H-J**) indicate values that are covered
328 used in the property data.
329
330 **Figure 4: Generalization to other ion channels.** Mean insertion fitness (**A**) and UMAP
331 insertion fitness classification (**B**) mapped onto the crystal structures of Kir2.2 (PDB 3SPI
332 (*21*); 70% identity with Kir2.1), Kir3.2 (PDB 4KFM (*23*); 45% identity with Kir3.1),

333 Kv1.2/Kv2.1 paddle chimera (PDB 2R9R (*24*), 62% identical with Kv1.3), $P2X_3$ (PDB
334 5SVK (*25*)), and Asic1a (PDB 6AVE (*26*)). N- and C-terminal residues not resolved in
335 crystal structures are modelled. For all channels apart from $P2X_3$, fitness classes describe
336 conformationally rigid and structured regions (class 1; cyan), highly flexible and
337 unstructured regions (class 2; red), and structured and dynamic regions (class 3; yellow)
338 that are often coincide with structural elements important for gating transition (dashed
339 circles). In $P2X_3$, there are two regions that separate rigid transmembrane helices and
340 ectodomain (class 1; cyan) and structured and dynamic regions (class 3; yellow). The
341 ligand ATP is shown in soft red.
342
343 **References**


344 1. C. Chothia, J. Gough, C. Vogel, S. A. Teichmann, *Science* **300**, 1701 (2003).
345 2. C. Y. Lin, J. C. Liu, *Curr Opin Biotechnol* **40**, 56 (2016).
346 3. S. Vishwanath, A. G. de Brevern, N. Srinivasan, *PLoS Comput Biol* **14**, e1006008
347 (2018).
348 4. W. Coyote-Maestas, Y. He, C. L. Myers, D. Schmidt, *Nat Commun* **10**, 290 (2019).
349 5. W. Coyote-Maestas, D. Nedrud, S. Okorafor, Y. He, D. Schmidt, *Nucleic Acids Res*
350 **48**, e11 (2020).
351 6. K. A. Matreyek, J. J. Stephany, M. A. Chiasson, N. Hasle, D. M. Fowler, *Nucleic*
352 *Acids Res* **48**, e1 (2020).
353 7. H. Hibino *et al.*, *Physiol Rev* **90**, 291 (2010).
354 8. D. M. Papazian, *Neuron* **23**, 7 (1999).
355 9. D. Ma *et al.*, *Science* **291**, 316 (2001).
356 10. D. Ma *et al.*, *Neuron* **33**, 715 (2002).
357 11. D. Ma *et al.*, *Cell* **145**, 1102 (2011).
358 12. C. Stockklausner, J. Ludwig, J. P. Ruppersberg, N. Klöcker, *FEBS Lett* **493**, 129
359 (2001).
360 13. J. L. Popot, D. M. Engelman, *Biochemistry* **29**, 4031 (1990).
361 14. K. Fallen *et al.*, *Channels (Austin)* **3**, 57 (2009).
362 15. L. McInnes, J. Healy, J. Melville, *arXiv preprint arXiv:1802.03426* (2018).

16. C. Xu, S. A. Jackson, *Genome Biol* **20**, 76 (2019).
17. S. Campioni *et al.*, *Nat Chem Biol* **6**, 140 (2010).
18. M. Munson *et al.*, *Protein Sci* **5**, 1584 (1996).
19. G. J. Rocklin *et al.*, *Science* **357**, 168 (2017).
20. O. Dagliyan *et al.*, *Science* **354**, 1441 (2016).
21. S. B. Hansen, X. Tao, R. MacKinnon, *Nature* **477**, 495 (2011).
22. E. M. Zangerl-Plessl *et al.*, *J Gen Physiol* **152**, (2020).
23. M. R. Whorton, R. MacKinnon, *Nature* **498**, 190 (2013).
24. S. B. Long, E. B. Campbell, R. Mackinnon, *Science* **309**, 897 (2005).
25. S. E. Mansoor *et al.*, *Nature* **538**, 66 (2016).
26. N. Yoder, C. Yoshioka, E. Gouaux, *Nature* **555**, 397 (2018).
27. L. Tu, J. Wang, A. Helm, W. R. Skach, C. Deutsch, *Biochemistry* **39**, 824 (2000).
28. D. El-Wahsch *et al.*, *Biophysical Journal* **102**, 58a (2012).
29. D. L. Minor *et al.*, *Cell* **102**, 657 (2000).
30. S. W. Lockless, R. Ranganathan, *Science* **286**, 295 (1999).
31. M. Gimona, *Nat Rev Mol Cell Biol* **7**, 68 (2006).

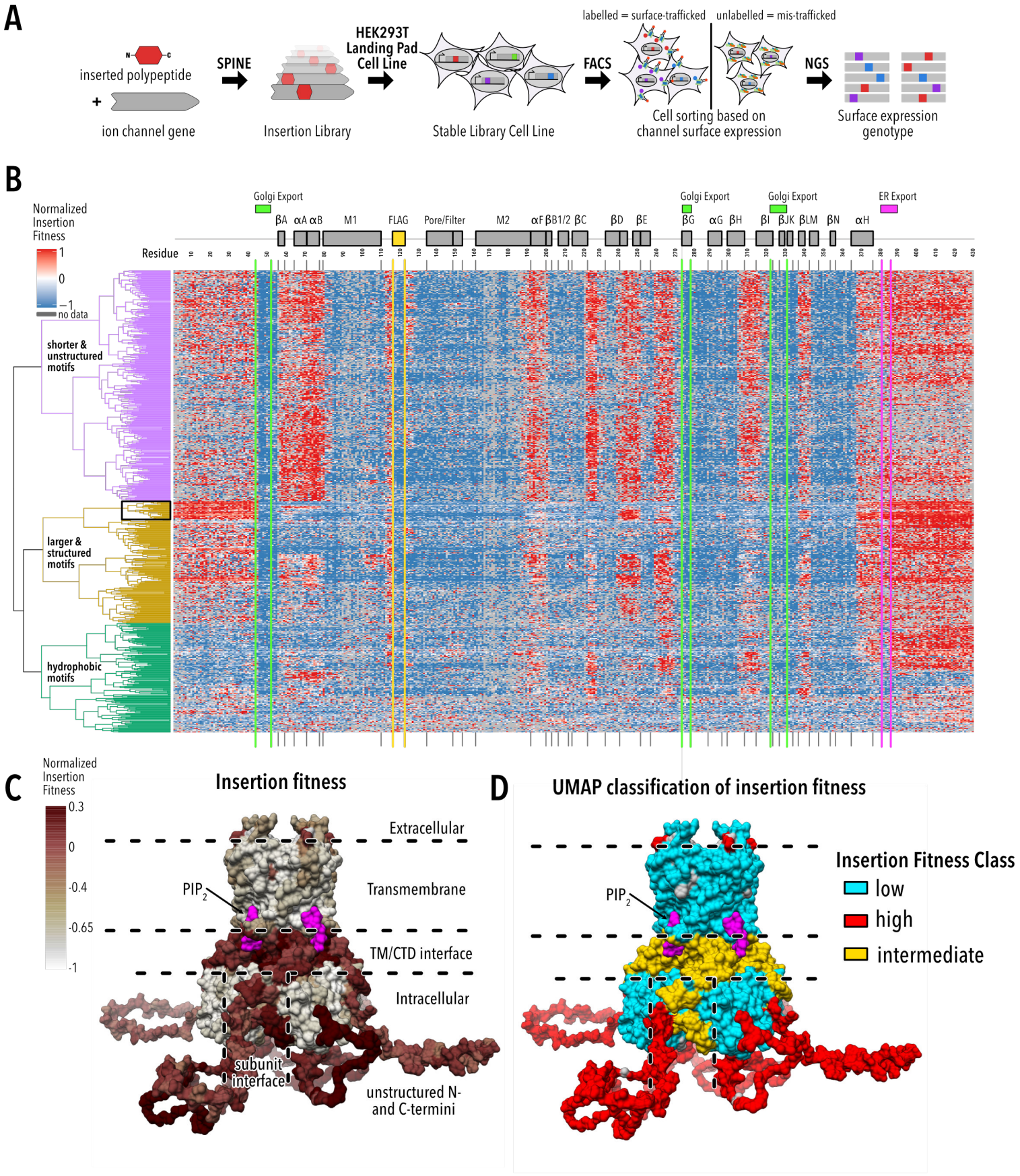
A
inserted polypeptide
+
ion channel gene
SPINE
Insertion Library
HEK293T Landing Pad Cell Line
Stable Library Cell Line
FACS
labelled = surface-trafficked
unlabelled = mis-trafficked
Cell sorting based on channel surface expression
NGS
Surface expression genotype
B
Normalized Insertion Fitness
1
0
−1
no data
Residue
Golgi Export
ER Export
βA αA αB M1 FLAG Pore/Filter M2 αF βB1/2 βC βD βE βG αG βH βI βJK βLM βN αH
shorter & unstructured motifs
larger & structured motifs
hydrophobic motifs
C
Normalized Insertion Fitness
0.3
0
-0.4
-0.65
-1
Insertion fitness
Extracellular
Transmembrane
TM/CTD interface
Intracellular
PIP2
subunit interface
unstructured N- and C-termini
D
UMAP classification of insertion fitness
Insertion Fitness Class
low
high
intermediate
PIP2

Figure 1

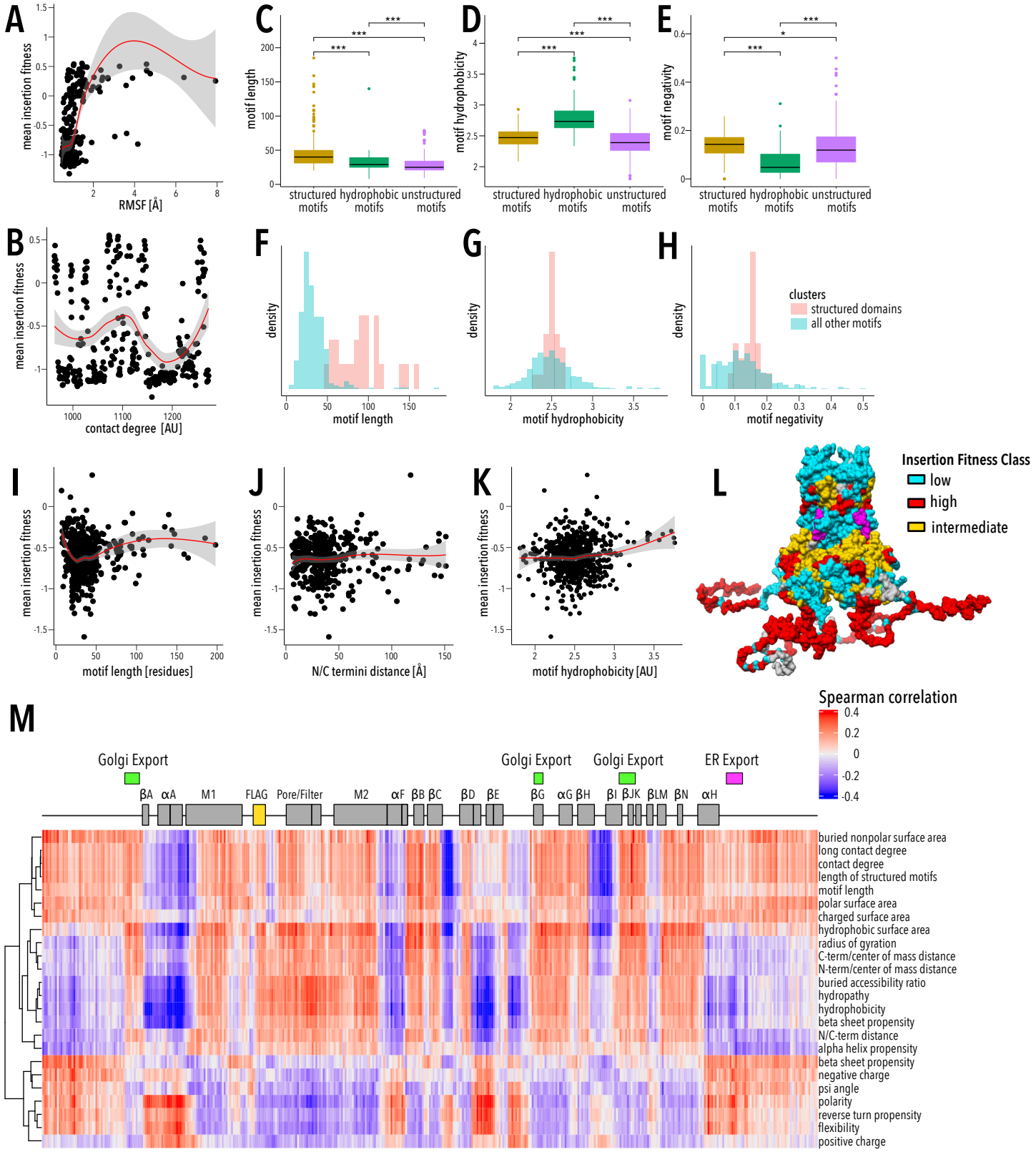
A
mean insertion fitness
RMSF [Å]
B
mean insertion fitness
contact degree [AU]
C
motif length
structured motifs
hydrophobic motifs
unstructured motifs
D
motif hydrophobicity
E
motif negativity
F
density
motif length
G
motif hydrophobicity
H
clusters
structured domains
all other motifs
motif negativity
I
motif length [residues]
J
N/C termini distance [Å]
K
motif hydrophobicity [AU]
L
Insertion Fitness Class
low
high
intermediate
M
Spearman correlation
Golgi Export
ER Export
βA αA M1 FLAG Pore/Filter M2 αF βB βC βD βE βG αG βH βI βJK βLM βN αH
buried nonpolar surface area
long contact degree
contact degree
length of structured motifs
motif length
polar surface area
charged surface area
hydrophobic surface area
radius of gyration
C-term/center of mass distance
N-term/center of mass distance
buried accessibility ratio
hydropathy
hydrophobicity
beta sheet propensity
N/C-term distance
alpha helix propensity
beta sheet propensity
negative charge
psi angle
polarity
reverse turn propensity
flexibility
positive charge

**Figure 2**

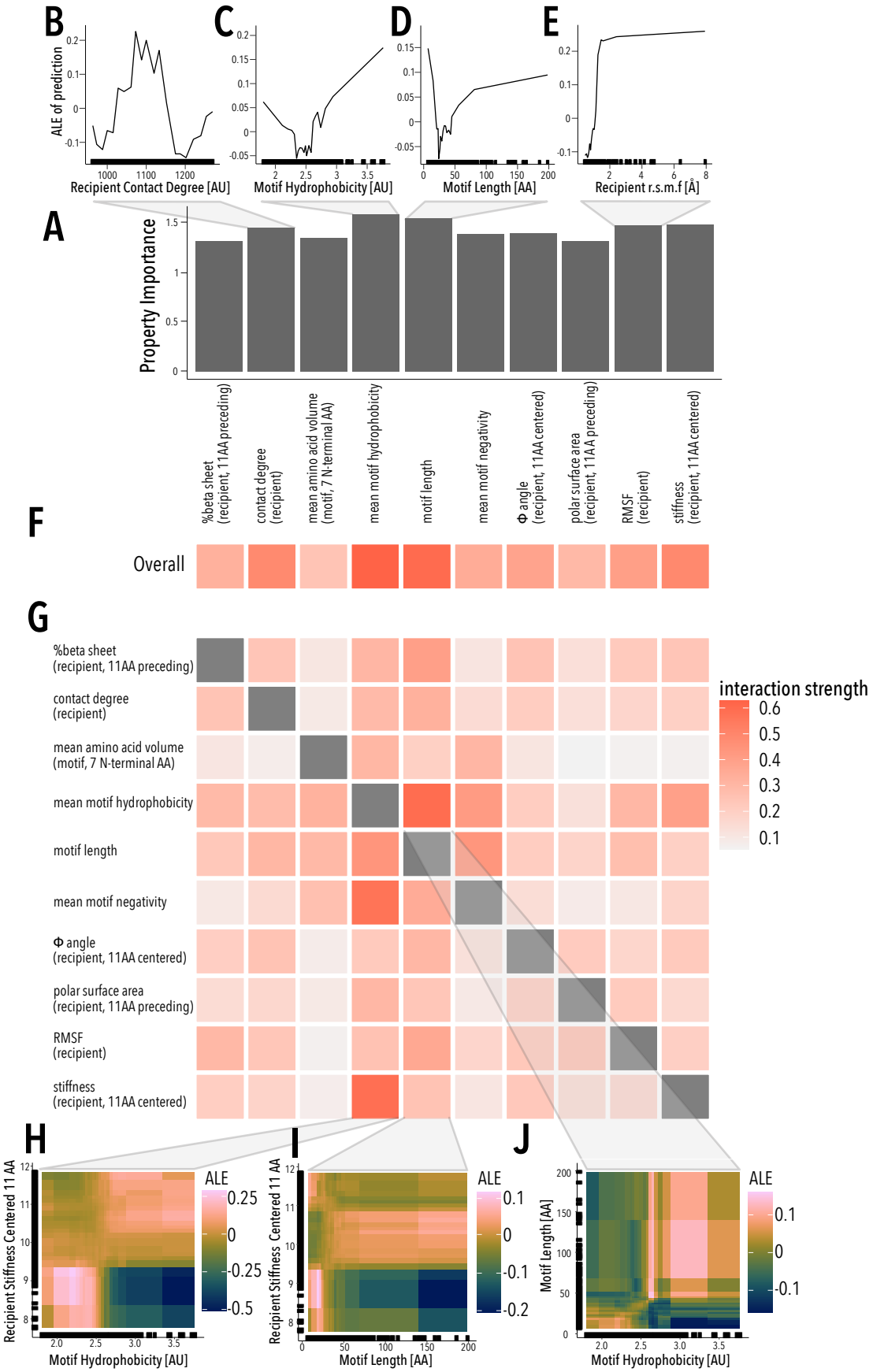
B
C
D
E
ALE of prediction
Recipient Contact Degree [AU]
Motif Hydrophobicity [AU]
Motif Length [AA]
Recipient r.s.m.f [Å]
A
Property Importance
%beta sheet (recipient, 11AA preceding)
contact degree (recipient)
mean amino acid volume (motif, 7 N-terminal AA)
mean motif hydrophobicity
motif length
mean motif negativity
Φ angle (recipient, 11AA centered)
polar surface area (recipient, 11AA preceding)
RMSF (recipient)
stiffness (recipient, 11AA centered)
F
Overall
G
interaction strength
H
I
J
Recipient Stiffness Centered 11 AA
Motif Hydrophobicity [AU]
Motif Length [AA]
ALE

**Figure 3**

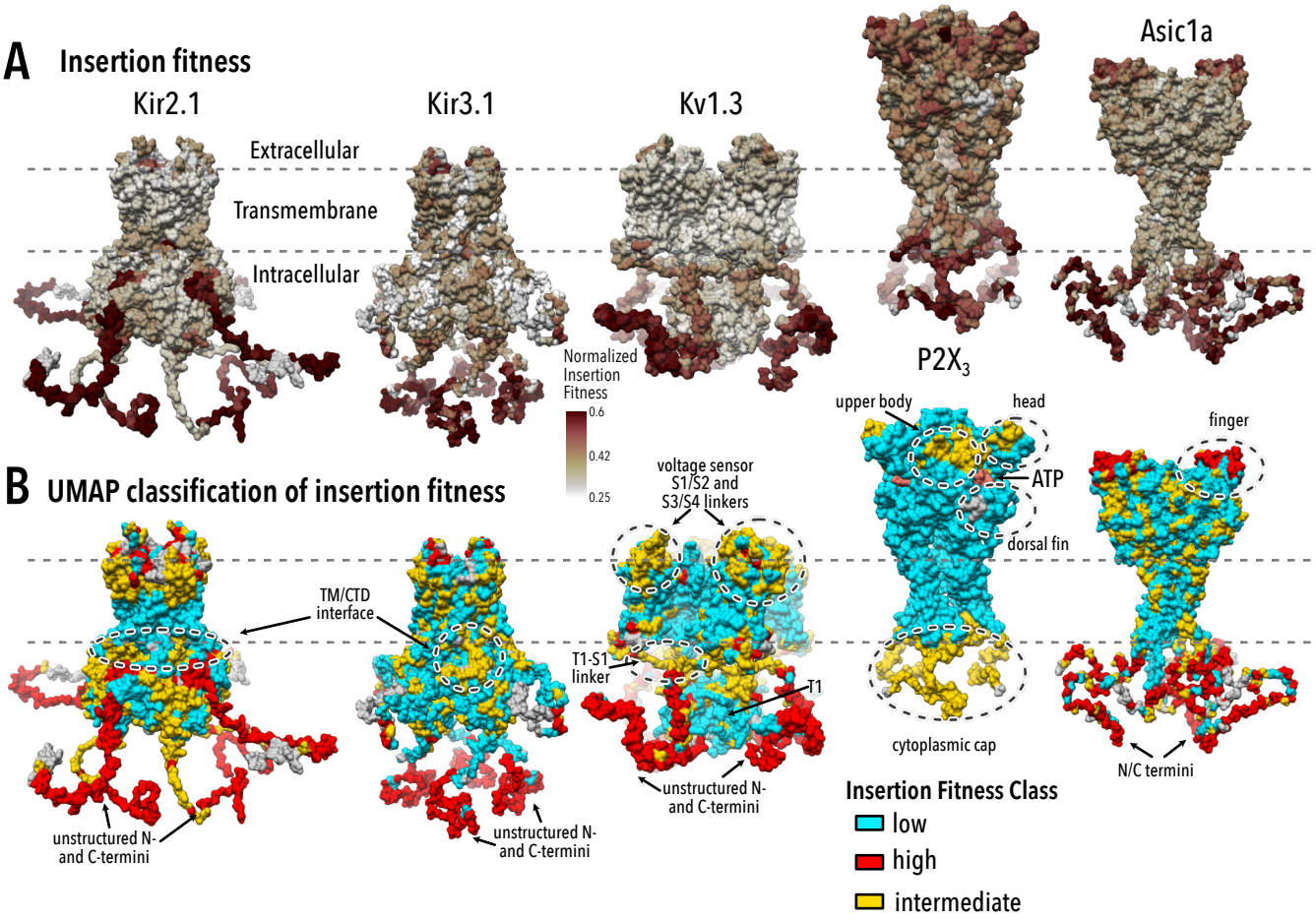
A
Insertion fitness
Kir2.1
Kir3.1
Kv1.3
Asic1a
Extracellular
Transmembrane
Intracellular
Normalized Insertion Fitness
0.6
0.42
0.25
P2X3
upper body
head
finger
ATP
dorsal fin
B
UMAP classification of insertion fitness
voltage sensor S1/S2 and S3/S4 linkers
TM/CTD interface
T1-S1 linker
T1
unstructured N- and C-termini
cytoplasmic cap
N/C termini
Insertion Fitness Class
low
high
intermediate

Figure 4

380 **Supplemental Materials**

381

382 **Material & Methods**

383 *Choice of domains:* We curated 760 motifs a representative sample of biophysical
384 properties that drive donor/recipient compatibility (**Supp. Table 1**). Common domains in
385 extant proteins are selected from SMART domain groups, focusing on those with
386 available structural information, and varying range of frequencies within the human
387 genome (*32*). The disordered protein fragments and proteins are from a curated
388 disordered protein database, DISPROT (*33*). The protein fragments are derived from
389 proteins with disordered regions, and the proteins are entire proteins that are disordered.
390 The manually curated motifs include natural, synthetic proteins, several switchable
391 proteins, and a flexible GSAG linker (**Supp. Table 5**). The polypeptide linkers are
392 manually selected hydrophobic and hydrophilic subsections from Kir2.1. Ancestral motifs
393 have been proposed by Alva et al. (*34*). The small non-domain proteins are manually
394 selected monomeric small proteins which are not commonly recombined. The smotifs are
395 super-secondary structural motifs that are common across proteins (*35*). The natural
396 proteins <50 AA acid motifs are a set of proteins under 50 amino acids that do not contain
397 cysteines that were used in a massive protein stability assay (*19*). Peptide toxins are a
398 set of genetically encodable disulfide-rich neurotoxin peptides.

399

400 *Molecular Biology:* Genes encoding human Kir2.1 (Uniprot P63252), human Kir3.1
401 (Uniprot P48549), human Kir3.2 (Uniprot P48051), human Asic1a (Uniprot P78348),
402 human $P2X_3$ (Uniprot P56373), and human Kv1.3 (Uniprot P22001) were produced by
403 DNA synthesis (Twist Bioscience). A Kozak sequence (GCCACC) and P2A-EGFP were
404 added prior and after each open reading frame, respectively. FLAG tag epitopes were
405 added into previous described extracellular loops of Kir2.1 (between S116 and K117
406 (*12*)), Kir3.1 (between K114 and A115 (*10*)), Asic1a (between F147 and K148 (*36*)), and
407 $P2X_3$ (between N72 and R73 based on insertion into paralog $P2X_2$ (*37*)). Golden Gate
408 compatible 5' and 3' sites where added to each gene by inverse PCR. Sequences of final
409 constructs are in **Supplemental Note 2**.

410

411 *Library generation:* We generated motif insertion libraries using Saturated Programmed
412 Insertional Engineering (SPINE) (*5*). Briefly, we use multi-step Golden Gate cloning to
413 insert a series of motifs in between all consecutive residue pairs of a gene. We break up
414 a gene into fragments (~169 bps or 53 amino acids) with a genetic handle cassette
415 inserted at every amino acid position. The genetic handle has outward-facing BsaI type
416 IIS restriction sites, which are replaced with any DNA fragment with short N-terminal Ser-
417 Gly and C-terminal Gly-Ser of the inserted motif. We include an antibiotic cassette,
418 Chloramphenicol, to remove background wildtype DNA and select for inserted library
419 members. As a quality control step, we sequence all our libraries for baseline coverage
420 prior to screens (**Supp. Fig. 20)**.
421

422 *Cloning domains:* The common domains, hand-curated motifs, and non-domain proteins
423 were ordered as gene fragments (Twist Bioscience). The disordered, gene fragments,
424 ancestral, structural, and motifs PDBs <50 amino acids were ordered in the form of an
425 OLS pool (Agilent). All motifs were mammalian codon optimized and designed with
426 amplifiable barcodes and BsaI type IIs restriction sites complementary to those in the
427 inserted genetic handle. Golden gate cloning is conducted with BsaI-v2 HF (NEB), T4
428 Ligase (NEB) following manufacturer's instructions. Completed Golden Gate reactions
429 were cleaned with Zymo Clean Concentrate kits and transformed into Lucigen E. cloni™
430 electrocompetent cells. Diversity was maintained at every step such that there are at least
431 30x successfully transformed colony forming units as determined by serial dilutions and
432 plating an aliquot of liquid cultures.
433

434 *Library cell line construction:* To generate cell lines, we used a rapid single-copy
435 mammalian cell line generation pipeline (*6*). Briefly, insertion libraries are cloned into a
436 staging plasmid with BxBI-compatible *attB* recombination sites using BsaI Golden Gate
437 cloning. We amplify the backbone using inverse PCR and the library of interest with
438 primers that add complementary BsaI cut sites. Golden Gate cloning is conducted with
439 BsaI-v2 HF (NEB), T4 Ligase (NEB) following manufacturer's instructions. Completed

440 Golden Gate reactions were cleaned with Zymo Clean Concentrate kits and transformed
441 into Lucigen E. cloni™ electrocompetent cells. Diversity was maintained at every step
442 such that there are at least 30x successfully transformed colony forming units as
443 determined by serial dilutions and plating an aliquot of liquid cultures. Completed library
444 landing pad constructs are co-transfected with a BxBI expression construct (pCAG-NLS-
445 Bxb1) into (TetBxB1BFP-iCasp-Blast Clone 12 HEK293T cells). This cell line has a
446 genetically integrated tetracycline induction cassette, followed by a BxBI recombination
447 site, and split rapalog inducible dimerizable Casp-9. Cell are maintained in D10 (DMEM,
448 10% w/v fetal bovine serum (FBS), 1% w/v sodium pyruvate, and 1% w/v
449 penicillin/streptomycin). Two days after transfection, doxycycline (2 ug/ml, Sigma-Aldrich)
450 is added to induce expression of our genes of interest (successful recombination) or the
451 icasp9 selection system (no recombination). Successful recombination shifts the iCasp-9
452 out of frame, thus only cells that have undergone recombination survive, while those that
453 haven't will die from iCasp-9-induced apoptosis. One day after doxycycline induction,
454 AP1903 (10 nM, MedChemExpress) is added to cause dimerization of Casp9 and
455 selectively kill cells without successful recombination. One day after AP1903-Casp9
456 selection, media is changed back to D10 + Doxycyline (2 ug/ml, Sigma-Aldrich) for
457 recovery. Two days after cells have recovered, cells are reseeded to enable normal cell
458 growth. Once cells reach confluency, library cells are frozen in glycerol stocks in aliquots
459 for assays.
460
461 *Sequencing-based surface expression assay:* To measure how inserted motifs disrupt
462 channel expression, we measured surface expression of all variants. We thawed glycerol
463 stocks of library cell lines into wells of a 6 well dish, swapped media the following day to
464 D10, grew cells to confluency, split once to ensure maximum cell health, and swapped
465 media for D10 + doxycycline (2 ug/ml, Sigma-Aldrich). Kir3.1 cannot homo-tetramerize
466 and therefore requires a co-expressed Kir3.2 or Kir3.4 inward rectifier to surface express
467 (*21*). For this reason, 48 hours prior to sorting Kir3.1 libraries, we transiently transfected
468 the stable Kir3.1 insertion library cell line with 2 ug Kir3.2-P2A-miRFP670 and 6ul
469 Turbofect per well of a 6 well plate. For all libraries except for Kv1.3, we detached cells

470 with 1 ml Accutase (Sigma-Aldrich), spun down and washed three times with FACS buffer
471 (2% FBS, 0.1% $NaN_3$, 1X PBS), incubated for 1-hour rocking at 4degC with a BV421 anti-
472 flag antibody (BD Bioscience), washed twice with FACS buffers, filtered with cell strainer
473 5 ml tubes (Falcon), covered with aluminum foil, and kept on ice for transfer to the flow
474 cytometry core. For Kv1.3, cells were detached and washed the same except after initial
475 washing cells were brought up in FACS buffer with Agitoxin-2-Cys-TAMRA (5nM,
476 Alomone), filtered with cell strainer 5 ml tubes, and brought to cell sorting facility on ice.
477 Before sorting, 5% of cells were saved as a control sample for sequencing prior to sorting.
478
479 All cells except for Kir3.1 were sorted into unlabeled and labeled (either BV421 or
480 Agitoxin-Cys-TAMRA) populations based on $EGFP^{high}/label^{low}$ and $EGFP^{high}/label^{high}$,
481 respectively. On a BD FACSAria II P69500132 cell sorter, EGFP fluorescence was
482 excited with a 488 nm laser and recorded with a 525/50 nm bandpass filter and 505 nm
483 long-pass filter. BV421 fluorescence was excited using a 405 nm laser and recorded with
484 a 450/50 nm bandpass filter, TAMRA fluorescence was excited using a 561 nm laser and
485 recorded with a 586/15 nm bandpass filter, and miRFP670 was excited with a 640 nm
486 laser and recorded with 670/30 nm bandpass filter.
487
488 All cells (expect those expressing Kir3.1) were gated on forward scattering area and side
489 scattering area to find whole cells, forward scattering width, and height to separate single
490 cells, EGFP for cells that expressed variants without errors (our library generation results
491 in single base pair deletions that will not have EGFP expression because deletions will
492 shift EGFP out of frame (*5*)), and label for surface expressed cells. Kir3.1 library cells
493 were gated on forward scattering area and side scattering area to find whole cells, forward
494 scattering width and height to separate single cells, miRFP670 5 times to get varying
495 levels of Kir3.2 co-expression, GFP for cells that expressed variants without errors, and
496 label for surface expressed cells. For simplicity, we only report Kir3.1 enrichment for one
497 level of Kir3.2 (Kir3.2 #4). The surface expression label gate boundaries were determined
498 based on unlabeled cells from the same population because controls tend to have non-

499 representative distributions. Examples of the gating strategy for each channel is depicted
500 in **Supplemental figures 14-18**.
501
502 $EGFP^{high}/label^{low}$ and $EGFP^{high}/label^{high}$ cells were collected into catch buffer (20% FBS,
503 0.1% $NaN_3$, 1x PBS. For larger pooled sublibrary samples, we collected between at least
504 100,000 to 500,00 cells per gate which is 8-35x coverage. 15,000 cells in both gates of a
505 Kir2.1 library with a small flexible ASGASGA linker was collected each day to normalize
506 all the pooled libraries. For smaller 15 motifs samples, we collected between 4,000-
507 50,000 of each sample/library pair which is ~10-120x coverage for all libraries. We find
508 the more disruptive an insertion the more difficult it is to collect sufficient surface-labeled
509 cells to reach 30x coverage. This means that our lower coverage is assuming all positions
510 are represented in surface expressed cells.
511
512 *Sequencing:* DNA from pre-sort control and sorted cells were extracted with Microprep
513 DNA kits (Zymo Research) and triple eluted with water. The elute was diluted such that
514 no more than 1.5ug of DNA is used per PCR reaction and amplified for 20 cycles of PCR
515 using Primestar GXL (Takara Clonetech), run on a 1% agarose gel, and gel purified.
516 Primers that bind outside the recombination site ensure leftover plasmid DNA from the
517 original cell line construction step is not amplified. Purified DNA was quantified using
518 Picogreen DNA quantification. Equal amounts by mass of each domain insertion sample
519 were pooled by cell sorting category and split into two domain sets per channel library set
520 to segregate highly similar motifs sequences. Final amplicon pools were as follows:
521 control, surface expression low 1, surface expression high 1, function low1, function high
522 1, surface expression low 2, surface expression high 2, function low 2, and function high
523 2. Pooled amplicons were prepared for sequencing using the Nextera XT sample
524 preparation workflow, and sequenced using Illumina Novaseq in 2x150bp mode. Read
525 count statistics are in **Supplemental Table 6**.
526
527 *Enrichment Calculations:* Forward and reverse reads were aligned individually using a
528 DIP-seq pipeline (*38*), slightly modified for SPINE compatibility and for updated python

529 packages. If both forward and reverse reads report an insertion, duplicated domain
530 insertion calls are removed to avoid artificially boosting counts. This pipeline results in
531 .csv spreadsheets indicating insertion position, direction, and whether it is in frame.
532
533 Surface expression enrichment was calculated by comparing the change in
534 $EGFP^{high}/label^{low}$ to $EGFP^{high}/label^{high}$. Enrichment calculation was based on Enrich2
535 software (*39*) and written in R. Only positions with reads in both $label^{low}$ and $label^{high}$
536 groups were used in enrichment calculations. For each cell group, the percentage of
537 reads at each position was calculated after adding 0.5 to assist positions with very small
538 counts. Enrichment was calculated by taking the natural logarithm of $EGFP^{high}/label^{high}$
539 percentage divided by the $EGFP^{high}/label^{low}$ percentage for each position (i).
540

541 $$Enrichment_i = \log \frac{0.5 + Count_High_i}{\sum_i^n 0.5 + Count_High_i} \Big/ \frac{0.5 + Count_Low_i}{\sum_i^n 0.5 + Count_Low_i}$$

542
543 All datasets were z-scored to an internal control flexible linker motif (AGSAGSA)
544 enrichment (separate for each sequencing subpool) by subtracting the average medium
545 enrichment and dividing by the standard deviation of the medium enrichment. Replicates
546 (r) were combined by a weighted average, which was calculated by a restricted maximum
547 likelihood estimate (M) and standard error (SE) using 50 Fisher scoring iterations.

548 $$Enrichment_i = \sum_r^n Enrichment_{i,r} * \frac{\sqrt{M_r + {SE_r}^2}}{\sum_r^n \sqrt{M_r + {SE_r}^2}}$$

549 Standard error was calculated assuming a Poisson distribution.
550

551 $SE_i$

552 $$= \sqrt{\frac{1}{Count_High_i + 0.5} + \frac{1}{Count_Low_i + 0.5} + \frac{1}{\sum_i^n 0.5 + Count_High_i} + \frac{1}{\sum_i^n 0.5 + Count_Low_i}}$$

553

554 All other positions are treated as NA and are not considered in further analysis (exclusion
555 criteria), except for correlations between datasets as removing data adds more noise than
556 treating NAs as 0s due to sampling.
557
558 *Data quality:* Inserting 760 motifs into 432 Kir2.1 positions yields a total theoretical library
559 diversity of 328,320 variants. Each sub-pooled library we generated and screened
560 encompassed 12,500 variants. Due to random variance, some datasets were incomplete
561 (**Supp. Fig. 1**). To make downstream analysis more robust, we only included motifs with
562 data (after exclusion criteria outlined in *Enrichment Calculations)* in >80% of positions.
563 This left us with 637 out of 760 motifs (further details in **Supp. Table 1**).
564
565 *Clustering:* All motif insertional profiling data was clustered by calculating a cosine
566 distance matrix and clustering it with Ward's hierarchical clustering method using the
567 hclust function in R with the 'ward.D2' method. Uniform Manifold Approximation Projection
568 (UMAP)-based clustering was done using the uwot R package using cosine or Euclidean
569 distance metrics, and a local neighborhood size of 10 sample points. Neighborhood size
570 influences how UMAP balances local versus global structure in the data. Within a range
571 of neighborhood sizes tested (2-50), our choice best conveys the broader structure of the
572 data.
573
574 *Ensemble Network Model:* To calculate dynamics of the recipient and motifs with
575 available PDBs, we used the Prody Python package (*40*). For this we used code from
576 from Golinski et al. (*41*) as a starting point kindly provided by Alexander Golinski and
577 Benjamin Hackel (University of Minnesota). We calculated mean stiffness of each
578 backbone based on weighted sums of normal modes from an Anisotropic Network Model
579 of vibration. We calculated summed recipient stiffness for varying lengths (1, 3, 5, 7, 9,
580 11 amino acids) before, centered on, and after an insertion position. Motif stiffness was
581 summed for the entire motif and for varying lengths of the N- and C-termini (1, 2, 3, 4, 5,
582 and 6 amino acids).
583

584 *Molecular dynamics simulations:* All-atom force-field based molecular dynamics
585 simulations were carried out to sample multi-μs trajectories. Our structural models
586 (agonist-bound PDB 3SPI and apo state PDB 3JYC (*21*)) are constituted by the channel
587 embedded in a bilayer of ~1300 POPC lipids hydrated by two slabs containing ~170,000
588 waters and ~600 KCl ion pairs, for a total of ~700,000 atoms. We first generated the
589 coordinates of the missing amino acids in the experimental structures (mostly located in
590 unstructured regions) using ROSETTA (for this purpose we generated 10,000 models
591 and kept the representative structure of the most populated cluster). We then used
592 charmm-gui (*42*) to model the bilayer and the aqueous compartment. Simulations are
593 being performed with the charmm36 force field (*43*) at a temperature of T=303.15K, using
594 the highly parallel computational code NAMD2.12 (*44*) on 280 processors cores from
595 Temple University's Owlsnest. Per-residue root mean squared fluctuations (RMSF) were
596 calculated by considering the position of the $C_\alpha$ atoms of each residue using the R bio3D
597 package (*45*).
598
599 *Amino acid scoring:* We calculated bioinformatic scores for amino acids using the
600 Quantiprot python package (*46*). For scores we used: molecular weight, surface area,
601 alpha helical propensity, beta sheet propensity, buried accessibility ratio propensity,
602 flexibility, hydropathy, hydrophobicity, negative charge, pKa, polarity, positive charge,
603 reverse turn propensity, and volume. These scores were calculated for both recipient and
604 donors. We calculated summed recipient scores for varying lengths before, centered on,
605 and after an insertion position (1, 3, 5, 7, 9, 11 amino acids). Motif sequence scores were
606 summed for the entire motif and for varying lengths of the N and C termini (1, 2, 3, 4, 5,
607 and 6 amino acids). Motif length was also included.
608
609 *Protein Structural Properties:* A series of properties were calculated with heavily modified
610 code previously used to calculate properties of protein domains kindly provided by
611 Alexander Golinski and Benjamin Hackel (*41*) that uses Pymol called from python scripts.
612 Recipient protein PDBs were trimmed of any ions, water, and other none protein of
613 interest molecules. Recipient protein phi, psi, contact degree, contact order, long contact

614 degree, secondary structure percentage, alpha helical percentage, beta sheet
615 percentage, nonpolar solvent accessible surface area (SASA), charged SASA, and
616 hydrophobic SASA. For each of these properties, we summed recipient structural scores
617 for varying lengths (1, 3, 5, 7, 9, 11 amino acids) before, centered on, and after an
618 insertion position. For motifs with structures, the mean phi angle, mean psi angle, radius
619 of gyration, distance between n and c termini, distance of N and C termini to center of
620 mass, motif size in Daltons, mean contact degree, mean contact order, mean long contact
621 degree, mean secondary structure percentage, mean alpha helical percentage, mean
622 beta sheet percentage, mean nonpolar SASA, mean charged SASA, mean hydrophobic
623 SASA, and RMSD if there were multiple conformers were calculated. In addition to mean
624 motif structural properties, N- and C-terminal varying lengths (1, 2, 3, 4, 5, and 6 amino
625 acids) sums were calculated for the phi angle, psi angle, contact degree, contact order,
626 long contact degree, secondary structure percentage, alpha helical percentage, beta
627 sheet percentage, nonpolar SASA, charged SASA, hydrophobic SASA, and RMSD.
628
629 *Choosing features to train Random Forest:* To allow for greater interpretability of our
630 Random Forest-based models, we filtered the input features for redundancy. Our
631 approach to reduce property redundancy was as follows: For motifs, we took the shortest
632 and longest N- and C-terminal features as well as the mean motif features. We identified
633 redundant motif properties by setting a +/- 0.8 correlation cutoff calculated between the
634 motif property and permissibility across all motifs for a given site. We chose the most
635 explanatory of highly correlated motif properties based on summed absolute correlative
636 value across all positions. For recipient properties, we took the longest and shortest of
637 each mean property before, centered and after the insertion position. We identified
638 redundant recipient properties by setting a +/- 0.8 correlation cutoff calculated between
639 the recipient property and permissibility across all positions for a given motif. We chose
640 the most explanatory of highly correlated recipient properties based on summed absolute
641 correlative value across all motifs. These steps reduced our recipient properties from 908
642 (520 recipient and 388 motif) properties down to 64 (32 recipient and 32 motif) properties.
643

644 *Random Forests:* Once we had a non-redundant set of 64 properties, we trained a
645 preliminary random forest model with 500 trees (**Supp. Fig. 5**). Based on this preliminary
646 model, we further trimmed the properties down to the most explanatory 20 (12 recipient
647 and 8 motif properties). We retrained the model without a significant drop in model
648 performance (39.98% variance explained for 69 properties and 39.44% for 20 properties,
649 **Supp. Table 4**). However, at this point we were including motif structural properties. This
650 meant that we were not able to include any motifs without structural data. As only 1 of
651 the top 10 most predictive properties ('Motif Phi Mean' as the 9$^{th}$ most predictive) were
652 from the structured domain set, we decided to exclude structure-based motif features
653 alltogether. This allowed us to include more motifs and reduce our non-redundant
654 properties set down further (39.44% variance explained for 20 properties and 38.69% for
655 10 properties, **Supp. Table 4**). We ended up choosing the top 10 most predictive features
656 which included 6 recipient features (stiffness, phi angle of 11 AA centered around
657 insertion site, MD simulation RMSF, contact degree at insertion site, polar surface area
658 of 11 AA preceding insertion site, beta sheet content in 11 AA preceding insertion site)
659 and 4 motif features (mean hydrophobicity, motif length, mean negative charge, mean
660 amino acid volume of 7 N-terminal residues). This final model was trained using 85% of
661 the data, with the other 15% withheld for testing, and performed well on the test dataset
662 (**Supp. Fig. 6**). All random forests were trained using the Randomforest package in R
663 with 500 trees and localimp = 'TRUE' with all model parameters set to default values.
664
665

**Supplemental Note 1: Detailed rules for protein recombination from machine learning.**

*Properties that guide recombination*: Random forest models allow us to study how a set of properties interact non-linearly to give rise to a phenotype. We trained a random forest model on a set of recipient and motif properties to learn what determines productive protein motif insertions into our recipient protein Kir2.1. We calculate feature importance for every property by looking at how model performance is impacted when a given property is not included in the model. We find the most important property overall is motif hydrophobicity, with recipient flexibility (stiffness and RMSF), motif length, and recipient space around an insertion site (contacts) close behind. The most important motif properties are the motifs length and hydrophobicity, and the most important recipient properties are contact degree and stiffness. However, based on feature importance alone, we do not know how properties relate to insertions.

We can further investigate how properties give rise to productive insertions through accumulated local effects (ALE) plots (**Figure 3B-E, Supp. Fig. 7**). These plots summarize the local effects of a property on the model's prediction. For example, flexibility appears to have switch-like interactions whereby, below a threshold rigidity, it is quite deleterious (**Fig. 3E, Supp. Fig. 7C** Positive relationship in RMSF and **Supp. Fig. 7G** negative relationship in stiffness). Other recipient properties also have straightforward positive or negative relationships such as polar solvent accessible surface area (SASA) (negative, **Supp. Fig. 7J**), beta sheet % (positive, **Supp. fig 7F**), and Phi angle (positive, **Supp. Fig. 7D**). Contact degree on the other hand has a nonlinear and non-monotonic interaction suggesting this recipient property is more complex (**Fig. 3B**, **Supp. Fig. 7E**). Overall, recipient features appear to determine insertional fitness in relatively simple ways, such as flexibility and beta sheets 11 amino acids prior to an insertion position are positive, which likely means flexible loops are desirable insertion positions. This result is in line with previous insertion strategies (*20*).

696 In contrast, all motif properties have more complex relationships to insertional fitness. For
697 example, lower motifs hydrophobicity appears to be deleterious (1.8-2.5) then becomes
698 beneficial at higher values. Similarly, motif length is negative until it becomes beneficial
699 in the model at about 25 amino acids. This is true for the other motif features as well:
700 motif negativity (**Supp. Fig. 7B**) is initially negative (albeit noisy) then becomes positive.
701 N-terminal 7 amino acid volume (**Supp. Fig. 7I**) that is initially positive, becomes negative,
702 and returns to be positive. Overall, this suggests motif properties have more complex
703 relationships to insertional fitness. Motif properties are beneficial in some contexts and
704 deleterious in others.
705
706 Taken together, recipient properties behave as expected in which flexible loops appear
707 to be beneficial. In contrast to existing approaches to engineer synthetic fusion protein
708 (e.g., (*20*)) that consider inserts to be interchangeable and solely focus on the properties
709 of insertion positions, we propose that inclusion of motifs properties and their interactions
710 is crucial to understand whether an insertions is viable at a given insertion position.
711
712 *Interactions between properties:* Random forests are comprised of many decision trees
713 built from random subsets of features that in aggregate predict a desired outcome from
714 properties. Decision trees make predictions by splitting a dataset at property thresholds
715 set on each input feature. Thresholds on multiple input features enable decision trees,
716 and by extension forests, to capture non-linear interactions between properties if they are
717 predictive of the class being modeled. These non-linear interactions are why a property
718 such as motif length can be positive and negative in different contexts.
719
720 To interpret why motif properties and contact density behave non-linearly, we explored
721 their interactions (**Fig. 3F-J, Supp. Figs. 8-10**). We find that motif hydrophobicity and
722 length interact substantially more than all other properties with recipient contact degree
723 and stiffness the next highest interactions (**Fig. 3F**). Motif properties having more
724 interactions than recipient properties makes sense in light of our earlier observation that

motif properties are more likely to non-linearly impact insertional fitness. However, just looking at overall interactions' strength does not tell us which features interact.

To identify which properties are interacting with which, we calculated pairwise interaction strengths between all properties (**Fig. 3G**). The strongest interactions overall in-order of strength are pairwise interactions between motif hydrophobicity with motif length, negativity, and stiffness. Overall, there are many pairwise interactions between all the motif features and limited interactions between motif and recipient properties. For recipient properties there are no strong interactions between recipient properties and very few interactions with motif features. That said, recipient stiffness interacts with motif hydrophobicity and length. There are also moderate pairwise interactions between recipient contact degree with hydrophobicity and motif length. Overall, this means that motif properties interact with each other to determine how a motif behaves when inserted into a position and secondarily with recipient properties to determine whether a motif feature set is beneficial.

To learn which interactions are driving insertional fitness, we calculated and plotted pairwise ALE. It is important to note that pairwise ALE only represents the interaction that contributes to insertional fitness and does not consider how either property contributes alone.

When looking at the strongest interaction overall, motif hydrophobicity and recipient stiffness it is apparent that very high hydrophobicity is extremely deleterious within very flexible regions, low hydrophobicity is very beneficial in flexible regions, and high hydrophobicity is moderately beneficial in stiff (likely buried) regions (**Fig. 3H**). Observing non-linear interactions help us build hypotheses of underlying biophysical mechanisms, such as hydrophobic residues when exposed and inserted into flexible surface exposed regions are extremely deleterious, whereas when these same motifs are inserted into buried likely more hydrophobic regions these become beneficial. In addition, interactions between motif length (> ~25 AA) and stiffness demonstrate a different trend, where long

755 insertions into very flexible regions are deleterious (these are regions at the termini of the
756 structure likely needed for folding and small flexible loops) and very rigid regions are also
757 deleterious for long motifs (**Fig 3I**). Whereas longer motifs are beneficial in intermediate
758 flexibility regions which are regions within the structured C-terminal domains that move
759 (e.g., flexible loops and the $PIP_2$ binding sites). By comparing these two pairwise ALEs
760 (**Fig. 3H** Stiffness-Hydrophobicity and **Fig. 3I** Stiffness-Length), we can see that short
761 non-hydrophobics are most preferred within very flexible regions, short hydrophobics are
762 most preferred within very flexible regions, and longer partially hydrophobic motifs are
763 preferred in semi-flexible regions. Furthermore, hydrophobicity is deleterious for short
764 motifs, beneficial for longer motifs, and extremely deleterious for short motifs (**Fig. 3J**).
765 Perhaps in longer motifs, hydrophobic residues provide stabilization by virtue of well-
766 formed hydrophobic cores, whereas shorter motifs lack well-formed hydrophobic cores
767 and instead expose hydrophobic residues thus becoming very disruptive by promoting
768 aggregation. Overall, this analysis points to motif hydrophobicity and length interacting to
769 determine how a motif behaves within the context of a recipient property. These
770 interactions give rise to the classes of motifs and regions, we observe in clustering **(Fig.**
771 **1B, D).**
772
773 To further investigate what drove specific motif cluster behavior, we investigated
774 calculated and annotated ALE plots based on where a motif class properties are located
775 (**Fig. 2C-E**).
776
777 *Unstructured short cluster behavior:* For the short unstructured motifs, non-hydrophobicity
778 and length are important within unstructured regions because these regions prefer polar
779 hydrophilic motifs as these will be solvent exposed (**Supp. Fig. 9B-D**). These motifs
780 however are not allowed well in buried regions based on high contacts being deleterious
781 for small motifs (**Supp. Fig. 9B, G**). In general negativity appears to play a weak negative
782 role (**Supp. Fig. 9E**). Finally, there is a strong beneficial interaction in regions with beta
783 sheets in the 11 amino acids preceding – perhaps implying flexible loops (**Supp. Fig. 9I,**
784 **J**). Flexible motifs are overwhelmingly inserted within flexible loops or at the termini of

785 beta sheets (**Supp. Fig. 9A**). This class is primarily best allowed within flexible and non-
786 buried regions. Motifs fall into this class if they are non-hydrophobic and small meaning
787 they will be non-disruptive from the perspective of space (contact degree), flexibility
788 (stiffness), and surface exposure (beta sheet %).
789
790 *Hydrophobic motifs:* For the hydrophobic motifs, it is quite clear that hydrophobicity drives
791 the behavior of this class. The motif length is not as important because hydrophobic motifs
792 range in size. Hydrophobic motifs mostly benefit from little negativity, which makes sense
793 as many hydrophobic motifs are best allowed with small segments of the transmembrane
794 M1 and negativity would be disruptive when interacting with lipids (**Supp. Fig. 10F**).
795 Hydrophobic motifs are very deleterious when inserted within very flexible regions and
796 beneficial within rigid regions (**Supp. Fig. 10B**). This combined with highly hydrophobic
797 motifs being beneficial within high contact regions (**Supp. Fig. 10G**) means hydrophobics
798 are beneficial when inserted within buried regions. Hydrophobics are highly deleterious
799 in and around beta sheets (**Supp. Fig. 10I**). Overall, this means hydrophobics behave
800 inversely to the unstructured short cluster. Hydrophobics are mostly deleterious but can
801 be inserted in some buried and transmembrane regions where they will not be disruptive.
802 That said, several recipient flexible loops can accept either motif class (βC-βD, βE-βG,
803 βH-βI, βL-βM). Interestingly, the βD-βE loop and unstructured termini that strongly allows
804 and prefers longer more structured motifs does not allow for most hydrophobic inserts,
805 perhaps because hydrophobics would interact with the solvent to cause misfolding and
806 aggregation.
807
808 *Larger structured motifs:* Larger more structured motifs contain nearly all folded proteins
809 and are most interesting from an engineering perspective. This class is overwhelmingly
810 determined by length, with hydrophobicity being intermediate and negativity only slightly
811 higher than other groups. While the overall class does appear to be driven by length,
812 length interacts strongly with hydrophobicity and weakly with negativity (**Supp. Fig. 8D-**
813 **E**). Hydrophobicity is positive for long motifs likely representing the ability to form a
814 hydrophobic core and fold. This interaction becomes even more clear when focusing on

815 a subset of motifs within this class that are commonly recombined domains and other well
816 folded larger proteins (**Supp. Fig. 8A,D**). There is a clear demarcation above which
817 hydrophobicity is highly beneficial (**Supp. Fig. 8D**), which is likely why folded proteins has
818 such a tight band of hydrophobicity (**Fig. 2G**). There is a similarly tight distribution of
819 negativity and may be an impact, but it is not nearly as strong (**Supp. Fig. 8E-F**). Large
820 motifs in very flexible (and generally small loops) large insertions are deleterious but
821 intermediate stiff regions are more amenable to larger insertions (**Supp. Fig. 8C**). That
822 space is a fundamental determinant for larger motifs is best illustrated by the interactions
823 with contact degree, where low contact degree is beneficial for the largest motifs (**Supp.**
824 **Fig. 8H**). Insertions of long motifs appear very deleterious in beta sheet rich regions,
825 which likely disrupt formation of the immunoglobulin-like C-terminal domain of Kir2.1
826 (**Supp. Fig. 8J**). Overall, motif length and hydrophobicity strongly interact positively to
827 give rise to increased insertional fitness likely through improving folding. Whether this is
828 beneficial is dependent on where an insertion occurs. Regions with some flexibility and
829 sufficient space are deleterious. However, if there is sufficient space (N -and C-termini
830 and βD-βE loop) insertions are actually quite beneficial. To better design domains for
831 recombination, it would be ideal to have stable domains that have sufficient size and
832 hydrophobicity to be able to maintain their fold after recombination, otherwise their folding
833 thermodynamics will likely be overruled by the recipient protein.

**Supplemental note 2:** Channel construct sequences

*Channel sequences:* All channel expression constructs were cloned directly downstream of a Kozak Sequence (GCCACC) and upstream of a P2A-EGFP. Unless otherwise noted, all were cloned into Landing Pad based staging plasmids 'attB-mcherry' from the Fowler and Matreyek labs where the mCherry was replaced with our genes of interest. Flag tag is bolded.

Kir2.1_Flag

ATGGGatcAGTGCGAACCAATCGGTATTCTATCGTATCAAGCGAGGAGGACGGGAT
GAAACTGGCAACCATGGCTGTAGCCAACGGTTTTGGGAATGGGAAATCTAAGGTG
CATACCCGCCAACAGTGCCGGTCACGCTTTGTCAAGAAAGATGGCCACTGTAATG
TGCAGTTCATAAACGTGGGGGAAAAGGGTCAACGGTACTTGGCCGATATTTTCACA
ACCTGCGTTGATATCCGCTGGCGCTGGATGTTGGTTATTTTTTGTCTCGCCTTCGT
ACTGTCTTGGCTCTTCTTTGGCTGCGTTTTTTGGTTGATCGCTTTGTTGCATGGAGA
TTTGGACACC**GATTATAAAGATGATGATGATAAA**TCCAAGGTATCCAAGGCCTGT
GTCTCCGAAGTAAATTCCTTTACCGCAGCTTTCCTTTTCTCTATCGAAACACAAACC
ACTATCGGATACGGGTTCCGATGCGTCACAGACGAATGCCCAATAGCCGTTTTCAT
GGTTGTCTTTCAATCAATAGTGGGCTGTATTATCGATGCATTTATCATTGGGGCCGT
GATGGCAAAAATGGCTAAGCCCAAAAAAAGAAATGAGACATTGGTTTTCAGTCACA
ACGCTGTGATTGCCATGAGGGATGGCAAGCTGTGCCTCATGTGGAGGGTGGGCA
ATCTGAGAAAGTCCCACCTCGTAGAGGCCCATGTACGAGCACAACTGCTGAAATC
ACGCATAACTTCAGAAGGAGAGTACATACCACTCGATCAGATTGATATCAATGTGG
GCTTCGATAGCGGCATTGACAGGATCTTTCTCGTTAGCCCAATCACCATCGTCCAC
GAGATTGATGAGGATTCTCCTCTTTATGACCTCTCCAAACAAGACATCGACAACGC
TGATTTCGAAATTGTCGTTATACTGGAAGGGATGGTAGAGGCCACCGCTATGACAA
CCCAATGTCGAAGTAGTTATCTTGCCAATGAAATCCTTTGGGGCCATCGCTACGAA
CCTGTCTTGTTTGAGGAGAAGCACTATTATAAGGTCGACTACTCTAGGTTCCACAA
AACATACGAAGTTCCTAACACACCATTGTGTAGTGCTCGGGACCTTGCAGAGAAGA
AGTACATTCTGTCTAACGCAAACTCTTTCTGTTACGAGAACGAAGTAGCTCTCACAT
CAAAGGAAGAAGAAGAAGATTCAGAGAACGGAGTTCCCGAGTCAACCAGCACCGA

CTCTCCTCCCGGCATTGACCTGCACAACCAAGCCAGTGTCCCCCTGGAGCCTAGA
CCTCTTCGGAGAGAGAGTGAAATCGCTGCTTCATCTGCAGTCAATGGGTCAGGC

Kir3.1_Flag
>ATGTCTGCACTTAGGCGGAAGTTCGGTGACGACTATCAGGTCGTGACCACATCCA
GTTCAGGATCTGGCCTTCAGCCACAAGGGCCTGGTCAAGGGCCACAACAACAGTT
GGTGCCAAAGAAGAAAAGACAGAGGTTCGTTGATAAGAACGGACGATGCAATGTT
CAGCACGGCAATCTCGGTAGTGAAACGTCACGCTATTTGTCTGATCTCTTCACCAC
CTTGGTAGACCTGAAATGGAGGTGGAACCTGTTTATATTCATCCTGACTTATACAGT
TGCTTGGCTCTTTATGGCTTCTATGTGGTGGGTTATAGCCTATACTAGAGGTGATCT
GAATAAAG**ACTATAAGGACGACGATGACAAA**GCTCATGTAGGGAATTATACTCCT
TGCGTCGCTAACGTCTACAATTTTCCTTCTGCCTTTCTGTTCTTCATAGAGACTGAG
GCTACCATTGGGTATGGATACAGGTATATAACCGACAAATGCCCTGAAGGCATTAT
TTTGTTTCTCTTTCAATCAATTTTGGGGTCTATTGTAGATGCATTCCTGATCGGGTG
TATGTTTATCAAAATGTCACAGCCTAAGAAGAGAGCTGAGACTTTGATGTTTTCCGA
GCATGCTGTCATTAGTATGAGGGATGGAAAATTGACTCTTATGTTCAGAGTAGGGA
ATCTCCGAAATTCACACATGGTCAGTGCCCAAATCCGGTGTAAACTTCTGAAGAGC
AGACAGACCCCAGAAGGGGAGTTTTTGCCTCTTGATCAGCTTGAATTGGATGTGG
GTTTTTCCACAGGCGCCGATCAGCTCTTCCTTGTAAGCCCACTGACCATTTGCCAT
GTCATCGACGCTAAAAGTCCCTTTTATGATCTGAGTCAGAGATCTATGCAGACTGA
ACAGTTTGAAGTTGTGGTGATATTGGAAGGTATTGTAGAGACTACTGGGATGACAT
GCCAAGCACGCACCTCTTATACCGAAGATGAAGTTTTGTGGGGACACCGATTTTTC
CCCGTGATCAGTCTTGAAGAGGGCTTTTTCAAAGTCGATTACTCTCAATTTCATGCT
ACTTTTGAGGTACCCACTCCACCTTACAGTGTTAAAGAACAAGAGGAAATGCTGCT
GATGAGCAGCCCCCTTATCGCACCCGCTATCACCAATTCTAAGGAGAGGCATAACT
CCGTTGAATGCCTCGATGGACTGGACGACATTTCTACTAAACTTCCATCAAAGTTG
CAGAAGATAACTGGGCGGGAGGATTTTCCTAAGAAATTGCTGAGGATGTCCTCCA
CAACTAGCGAAAAAGCATATAGTCTTGGTGACCTGCCCATGAAATTGCAAAGGATT
TCAAGCGTTCCTGGTAATTCAGAAGAAAAGCTCGTTAGTAAGACTACCAAAATGCT
GTCCGACCCTATGTCTCAAAGTGTTGCAGACTTGCCACCTAAACTTCAAAAGATGG

894 CAGGAGGCCCTACTAGAATGGAAGGGAATTTGCCAGCCAAGCTGCGCAAAATGAA
895 CTCCGACAGATTCACC
896
897 ASIC1a_Flag
898 ATGGAATTGAAAGCCGAAGAGGAAGAGGTCGGAGGTGTTCAACCAGTTTCTATCC
899 AAGCATTCGCCTCAAGTTCCACTTTGCACGGGTTGGCACACATATTCTCTTACGAA
900 CGCCTCAGCCTCAAACGAGCTCTTTGGGCTCTTTGCTTTCTGGGGTCACTTGCTGT
901 TCTTCTTTGCGTTTGTACCGAAAGGGTTCAGTATTATTTCCATTATCATCATGTTACT
902 AAACTCGACGAAGTCGCCGCATCACAGTTGACCTTCCCTGCTGTAACCCTTTGCAA
903 TCTGAACGAATTTAGATTTAGCCAAGTTTCTAAAAACGATCTCTATCACGCCGGTGA
904 ACTTCTCGCCCTCTTGAATAATCGCTATGAGATTCCCGATACACAAATGGCAGATG
905 AAAAGCAACTGGAGATCCTCCAGGATAAGGCCAACTTTCGGTCCTTC**GATTATAAA**
906 **GATGATGATGATAAA**AAGCCCAAGCCCTTCAATATGCGAGAGTTTTACGATCGCG
907 CTGGCCATGATATTCGGGATATGCTTCTCTCATGCCACTTCAGGGGGGAGGTTTGT
908 TCCGCAGAGGACTTCAAGGTCGTGTTTACCCGCTACGGCAAGTGTTATACCTTCAA
909 CAGCGGTCGCGACGGGCGCCCTCGGCTTAAAACCATGAAAGGCGGCACTGGTAA
910 CGGACTCGAAATCATGCTGGACATCCAACAAGATGAATACCTCCCCGTGTGGGGT
911 GAAACAGATGAAACCAGTTTCGAAGCTGGTATAAAGGTACAAATACATAGCCAAGA
912 TGAGCCCCCCTTTATTGACCAACTTGGCTTCGGTGTAGCACCCGGATTCCAGACAT
913 TTGTGGCCTGTCAAGAACAAAGGTTGATATATCTGCCCCCTCCCTGGGGGACCTGT
914 AAGGCCGTAACAATGGACTCCGACCTGGACTTTTTTGACTCCTACTCCATAACAGC
915 TTGTCGAATTGACTGTGAAACTAGATATCTTGTCGAGAATTGTAACTGTAGGATGGT
916 TCACATGCCCGGAGATGCCCCATACTGCACTCCCGAACAATACAAGGAGTGTGCC
917 GACCCTGCACTTGACTTTCTCGTTGAAAAAGATCAGGAGTATTGCGTGTGCGAGAT
918 GCCCTGTAATCTTACACGGTACGGTAAGGAACTTAGTATGGTCAAAATTCCAAGTA
919 AAGCCAGTGCAAAATACTTGGCTAAGAAGTTCAACAAAAGCGAGCAGTACATCGGC
920 GAGAACATTTTGGTTCTCGACATATTCTTCGAAGTCCTGAACTACGAAACTATTGAA
921 CAGAAAAAGGCATACGAGATAGCAGGTCTTTTGGGAGACATAGGAGGGCAGATGG
922 GGCTGTTTATAGGGGCTTCTATTCTGACTGTACTCGAACTGTTTGACTACGCTTATG
923 AAGTCATTAAACACAAGCTGTGTCGCCGCGGGAAATGTCAGAAGGAGGCTAAGAG

924 AAGCTCAGCCGATAAAGGCGTAGCTCTGTCTTTGGATGATGTAAAACGCCATAATC
925 CTTGCGAATCTCTTCGCGGGCACCCAGCCGGCATGACTTACGCCGCAAACATCCT
926 GCCCCATCATCCCGCACGAGGCACCTTCGAAGATTTTACATGTGCTGCCAGCTCT
927 GCTGTGAATGGTTCTGGA
928
929 P2X3_flag
930 ATGAATTGCATAAGTGATTTTTTTACCTACGAAACCACGAAGAGTGTAGTAGTCAAA
931 AGTTGGACGATAGGAATCATAAACCGCGTCGTACAATTGCTGATTATCTCATACTTT
932 GTAGGCTGGGTTTTTCTGCATGAAAAAGCATACCAAGTTAGGGATACGGCCATTGA
933 GTCATCAGTAGTCACGAAAGTCAAGGGCAGCGGCCTGTACGCTAAC**GATTACAAG**
934 **GACGACGATGACAAG**AGGGTTATGGATGTGAGTGATTATGTGACGCCCCCACAG
935 GGGACCAGCGTCTTTGTCATAATAACCAAAATGATAGTGACGGAAAATCAAATGCA
936 GGGCTTCTGTCCCGAGTCCGAGGAGAAATACCGATGTGTAAGTGACTCCCAGTGC
937 GGGCCTGAACGCCTCCCTGGTGGTGGTATCCTTACAGGTCGGTGCGTGAATTATT
938 CAAGTGTGCTGCGGACCTGTGAAATCCAGGGATGGTGTCCAACTGAGGTAGACAC
939 AGTCGAGACTCCTATCATGATGGAGGCAGAGAACTTCACTATCTTTATTAAGAACT
940 CTATACGCTTTCCACTGTTTAATTTTGAGAAGGGTAATCTTCTGCCAAACTTGACCG
941 CACGAGATATGAAAACATGTAGATTTCATCCGGACAAAGATCCTTTCTGCCCAATTC
942 TCCGCGTTGGAGATGTGGTGAAATTTGCTGGCCAGGACTTTGCAAAGCTGGCACG
943 CACGGGAGGTGTGTTGGGCATAAAAATTGGCTGGGTTTGTGACTTGGACAAGGCC
944 TGGGACCAGTGTATTCCCAAATATTCTTTTACAAGGCTGGACTCAGTATCAGAGAA
945 ATCAAGCGTGTCACCCGGTTATAACTTTCGGTTCGCTAAATACTACAAGATGGAGA
946 ACGGTTCAGAGTATCGCACCTTGCTGAAGGCGTTTGGTATTCGGTTTGATGTGCTC
947 GTTTACGGTAACGCGGGGAAGTTCAACATTATACCGACGATCATTAGCTCCGTGGC
948 CGCTTTTACTTCCGTTGGAGTCGGCACTGTTCTTTGCGATATCATCCTTCTGAATTT
949 TTTGAAAGGAGCCGATCAGTACAAGGCGAAAAAGTTCGAGGAAGTCAATGAAACG
950 ACGCTGAAAATTGCAGCGTTGACAAACCCTGTTTATCCAAGCGATCAAACAACAGC
951 GGAGAAACAGTCCACAGACTCTGGCGCATTTTCTATCGGGCAC
952
953 Kv1.3

954 ATGGACGAGCGGCTCAGTCTACTTCGCTCACCACCACCCCCCTCTGCTCGGCATC
955 GGGCCCATCCCCCTCAACGGCCAGCAAGCAGCGGCGGCGCACACACCTTGGTCA
956 ATCACGGGTACGCCGAGCCCGCTGCTGGCAGGGAACTTCCTCCAGACATGACCG
957 TCGTGCCTGGCGACCATCTTCTTGAACCCGAAGTGGCAGACGGCGGCGGCGCTC
958 CACCCCAGGGGGGCTGTGGAGGCGGAGGATGCGATCGGTATGAGCCATTGCCCC
959 CCTCCCTTCCAGCTGCCGGCGAGCAAGACTGCTGTGGGGAAAGAGTCGTCATAAA
960 CATTAGCGGGCTTCGATTCGAGACACAGCTTAAGACACTTTGTCAATTTCCAGAAA
961 CTCTTCTTGGGGACCCAAAACGCCGGATGCGGTATTTCGACCCCCTTAGAAACGA
962 ATACTTTTTTGATCGCAATAGGCCCAGTTTCGACGCCATCCTCTATTACTATCAGAG
963 CGGCGGGCGAATCCGCCGACCTGTCAATGTACCTATCGATATCTTTTCCGAAGAG
964 ATCAGGTTTTACCAGCTGGGAGAGGAAGCCATGGAGAAATTTCGCGAGGACGAGG
965 GGTTTCTGAGAGAAGAGGAACGCCCCCTCCCACGAAGGGATTTCCAGCGACAAGT
966 CTGGCTGTTGTTTGAGTACCCAGAGTCCTCAGGGCCCGCTCGAGGGATAGCAATC
967 GTGAGTGTCCTTGTTATTCTGATTAGTATAGTCATCTTTTGTCTTGAAACACTGCCA
968 GAATTTCGCGATGAGAAGGATTACCCAGCCTCAACTAGCCAGGACTCATTCGAGG
969 CAGCTGGCAATTCAACAAGCGGGAGCCGGGCAGGTGCATCTTCTTTCTCAGATCC
970 TTTTTTTGTTGTAGAAACACTCTGTATCATTTGGTTCAGTTTTGAATTGTTGGTAAGG
971 TTTTTCGCATGTCCCTCCAAGGCAACATTCTCCCGAAACATTATGAACCTGATTGAT
972 ATTGTCGCTATAATACCTTACTTCATCACCCTTGGTACTGAGTTGGCAGAGAGGCA
973 AGGCAATGGGCAGCAAGCCATGTCTTTGGCAATCCTCCGGGTCATCCGGCTTGTG
974 AGGGTTTTTAGGATCTTTAAATTGAGTCGGCATTCAAAAGGGCTCCAGATCCTTGG
975 TCAAACTTTGAAGGCTTCTATGAGAGAACTCGGGCTTCTTATATTTTTTCTCTTCATA
976 GGAGTTATTCTGTTTAGCAGTGCTGTGTATTTCGCTGAGGCCGATGATCCTACATC
977 TGGCTTTTCATCAATACCTGACGCATTTTGGTGGGCTGTTGTGACCATGACCACCG
978 TTGGTTACGGTGATATGCACCCCGTGACAATTGGCGGTAAAATCGTGGGCAGCCT
979 CTGTGCAATCGCTGGAGTATTGACCATCGCACTCCCAGTTCCCGTTATTGTTTCCA
980 ACTTTAATTACTTCTACCACAGAGAAACCGAGGGAGAAGAACAGAGCCAGTATATG
981 CACGTTGGCTCCTGTCAGCATTTGTCATCAAGTGCCGAGGAATTGCGAAAGGCTC
982 GGTCTAACAGCACCCTGTCCAAGAGTGAGTACATGGTTATCGAGGAGGGAGGTAT
983 GAATCATAGCGCTTTCCCCCAGACCCCTTTTAAAACTGGCAACTCTACTGCCACAT

984 GCACCACCAACAATAATCCAAACTCCTGCGTCAACATCAAGAAAATATTTACAGAC
985 GTG
986
987 Kir3.2 was used but with miRFP670 instead of EGFP and in a transient expression
988 backbone from pEGFPN3.
989 ATGACAATGGCTAAGTTGACCGAAAGTATGACTAACGTGCTTGAGGGGGACTCCAT
990 GGATCAGGATGTGGAGTCACCAGTTGCCATTCACCAGCCTAAGCTGCCCAAACAG
991 GCAAGGGACGACCTCCCTCGACACATATCACGGGATCGCACTAAGAGAAAGATAC
992 AAAGGTATGTAAGGAAAGACGGGAAGTGTAATGTCCATCACGGGAACGTGAGGGA
993 GACATATCGATACTTGACTGATATCTTCACTACACTGGTGGATCTCAAATGGAGGTT
994 CAATCTGCTCATATTTGTCATGGTTTATACCGTCACCTGGCTTTTTTTCGGTATGAT
995 CTGGTGGCTCATAGCATATATACGGGGGGATATGGACCATATAGAGGACCCATCA
996 TGGACTCCTTGCGTTACAAATCTCAACGGCTTTGTCTCCGCCTTTTTGTTCTCAATT
997 GAAACCGAGACTACAATCGGCTATGGGTACAGGGTCATTACTGACAAGTGTCCCG
998 AAGGTATCATCCTTCTTTTGATACAATCTGTACTCGGCAGTATTGTTAATGCATTCAT
999 GGTTGGCTGCATGTTCGTGAAAATATCCCAGCCCAAAAAAAGGGCTGAGACATTG
1000 GTGTTCTCAACTCACGCAGTAATTTCAATGAGAGATGGCAAGCTCTGTCTTATGTTT
1001 CGGGTAGGGGACCTTCGCAACAGCCACATCGTAGAGGCTAGCATCCGGGCAAAA
1002 CTTATTAAAAGTAAACAGACCAGTGAGGGCGAGTTCATCCCCCTGAACCAGAGTGA
1003 CATCAACGTGGGATATTATACCGGCGACGATCGCCTGTTTCTCGTTTCACCACTTA
1004 TAATATCTCATGAGATCAATCAGCAGAGCCCCTTTTGGGAGATTAGCAAAGCCCAA
1005 CTCCCTAAGGAAGAGCTTGAGATAGTGGTTATATTGGAAGGAATTGTCGAAGCAAC
1006 AGGGATGACATGTCAGGCACGGTCCAGTTATATTACATCTGAGATCCTCTGGGGG
1007 TACCGGTTTACCCCCGTTTTGACCATGGAAGATGGATTTTATGAGGTCGACTATAAT
1008 AGTTTTCACGAAACATACGAGACAAGCACACCTTCTCTTTCAGCTAAAGAGTTGGC
1009 TGAGTTGGCAAACCGGGCAGAAGTCCCACTTTCCTGGAGCGTGTCTAGCAAGCTG
1010 AATCAGCACGCTGAGTTGGAAACCGAGGAAGAGGAGAAGAATCCAGAAGAACTGA
1011 CTGAGCGGAATGGTGATGTGGCAAATCTCGAGAACGAGTCAAAGGTT
1012
1013 >P2A Sequence used

1014 GCAACTAATTTTAGTCTACTGAAACAAGCTGGTGATGTGGAGGAAAATCCAGGACC
1015 A
1016
1017 >EGFP Sequence Used
1018 atggtgagcaagggcgaggagctgttcaccggggtggtgcccatcctggtcgagctggacggcgacgtaaacggccac
1019 aagttcagcgtgtccggcgagggcgagggcgatgccacctacggcaagctgaccctgaagttcatctgcaccaccggc
1020 aagctgcccgtgccctggcccaccctcgtgaccaccctgacctacggcgtgcagtgcttcagccgctaccccgaccacat
1021 gaagcagcacgacttcttcaagtccgccatgcccgaaggctacgtccaggagcgcaccatcttcttcaaggacgacggc
1022 aactacaagacccgcgccgaggtgaagttcgagggcgacaccctggtgaaccgcatcgagctgaagggcatcgactt
1023 caaggaggacggcaacatcctggggcacaagctggagtacaactacaacagccacaacgtctatatcatggccgaca
1024 agcagaagaacggcatcaaggtgaacttcaagatccgccacaacatcgaggacggcagcgtgcagctcgccgacca
1025 ctaccagcagaacacccccatcggcgacggccccgtgctgctgcccgacaaccactacctgagcacccagtccgccct
1026 gagcaaagaccccaacgagaagcgcgatcacatggtcctgctggagttcgtgaccgccgccgggatcactctcggcat
1027 ggacgagctgtacaagtaa
1028
1029 >miRFP670
1030 aTGgTAGCAGGTCATGCCTCTGGCAGCCCCGCATTCGGGACCGCCTCTCATTCGA
1031 ATTGCGAACATGAAGAGATCCACCTCGCCGGCTCGATCCAGCCGCATGGCGCGCT
1032 TCTGGTCGTCAGCGAACATGATCATCGCGTCATCCAGGCCAGCGCCAACGCCGCG
1033 GAATTTCTGAATCTCGGAAGCGTACTCGGCGTTCCGCTCGCCGAGATCGACGGCG
1034 ATCTGTTGATCAAGATCCTGCCGCATCTCGATCCCACCGCCGAAGGCATGCCGGT
1035 CGCGGTGCGCTGCCGGATCGGCAATCCCTCTACGGAGTACTGCGGTCTGATGCAT
1036 CGGCCTCCGGAAGGCGGGCTGATCATCGAACTCGAACGTGCCGGCCCGTCGATC
1037 GATCTGTCAGGCACGCTGGCGCCGGCGCTGGAGCGGATCCGCACGGCGGGTTCA
1038 CTGCGCGCGCTGTGCGATGACACCGTGCTGCTGTTTCAGCAGTGCACCGGCTACG
1039 ACCGGGTGATGGTGTATCGTTTCGATGAGCAAGGCCACGGCCTGGTATTCTCCGA
1040 GTGCCATGTGCCTGGGCTCGAATCCTATTTCGGCAACCGCTATCCGTCGTCGACT
1041 GTCCCGCAGATGGCGCGGCAGCTGTACGTGCGGCAGCGCGTCCGCGTGCTGGTC
1042 GACGTCACCTATCAGCCGGTGCCGCTGGAGCCGCGGCTGTCGCCGCTGACCGGG
1043 CGCGATCTCGACATGTCGGGCTGCTTCCTGCGCTCGATGTCGCCGTGCCATTTAC

AATTCCTGAAGGACATGGGCGTGCGCGCCACCCTGGCGGTGTCGCTGGTGGTCG
GCGGCAAGCTGTGGGGCCTGGTTGTCTGTCACCATTATCTGCCGCGCTTCATCCG
TTTCGAGCTGCGGGCGATCTGCAAACGGCTCGCCGAAAGGATCGCGACGCGGAT
CACCGCGCTTGAGAGCTAA

1050 **Supplemental References**


1051 32. I. Letunic, P. Bork, *Nucleic Acids Res* **46**, D493 (2018).

1052 33. M. Sickmeier *et al.*, *Nucleic Acids Res* **35**, D786 (2007).

1053 34. V. Alva, J. Söding, A. N. Lupas, *Elife* **4**, e09410 (2015).

1054 35. G. Pugalenthi, P. N. Suganthan, R. Sowdhamini, S. Chakrabarti, *Bioinformatics* **23**,
1055 637 (2007).

1056 36. X. Chen, S. Gründer, *J Physiol* **579**, 657 (2007).

1057 37. E. Richler, E. Shigetomi, B. S. Khakh, *J Neurosci* **31**, 16716 (2011).

1058 38. D. C. Nadler, S. A. Morgan, A. Flamholz, K. E. Kortright, D. F. Savage, *Nat*
1059 *Commun* **7**, 12266 (2016).

1060 39. A. F. Rubin *et al.*, *Genome Biol* **18**, 150 (2017).

1061 40. A. Bakan, L. M. Meireles, I. Bahar, *Bioinformatics* **27**, 1575 (2011).

1062 41. A. W. Golinski, P. V. Holec, K. M. Mischler, B. J. Hackel, *ACS Comb Sci* **21**, 323
1063 (2019).

1064 42. S. Jo, T. Kim, V. G. Iyer, W. Im, *J Comput Chem* **29**, 1859 (2008).

1065 43. J. Huang, A. D. MacKerell, *J Comput Chem* **34**, 2135 (2013).

1066 44. J. C. Phillips *et al.*, *J Comput Chem* **26**, 1781 (2005).

1067 45. B. J. Grant, A. P. Rodrigues, K. M. ElSawy, J. A. McCammon, L. S. Caves,
1068 *Bioinformatics* **22**, 2695 (2006).

1069 46. B. M. Konopka, M. Marciniak, W. Dyrka, *BMC Bioinformatics* **18**, 339 (2017).

1070 47. M. Charrad, N. Ghazzali, V. Boiteau, A. Niknafs, J Stat Softw. (2014).

1071 48. D. A. Doyle et al., Cell 85, 1067 (1996).

1072 49. A. Taslimi et al., Nat Chem Biol 12, 425 (2016).

1073 50. M. Iwakura, T. Nakamura, Protein Eng 11, 707 (1998).

1074 51. M. Iwamoto, T. Björklund, C. Lundberg, D. Kirik, T. J. Wandless, Chem Biol 17,
1075 981 (2010).

1076 52. Y. He, Y. Chen, P. A. Alexander, P. N. Bryan, J. Orban, Structure 20, 283 (2012).

1077 53. G. Bhardwaj et al., Nature 538, 329 (2016).

1078 54. O. Dagliyan et al., Proc Natl Acad Sci U S A 110, 6800 (2013).

1079 55. A. S. Halavaty, K. Moffat, Biochemistry 46, 14001 (2007).

1080 56. M. Pazgier et al., Proc Natl Acad Sci U S A 106, 4665 (2009).
1081 57. B. Kuhlman et al., Science 302, 1364 (2003).
1082 58. E. Marcos et al., Science 355, 201 (2017).
1083 59. E. Marcos et al., Nat Struct Mol Biol 25, 1028 (2018).

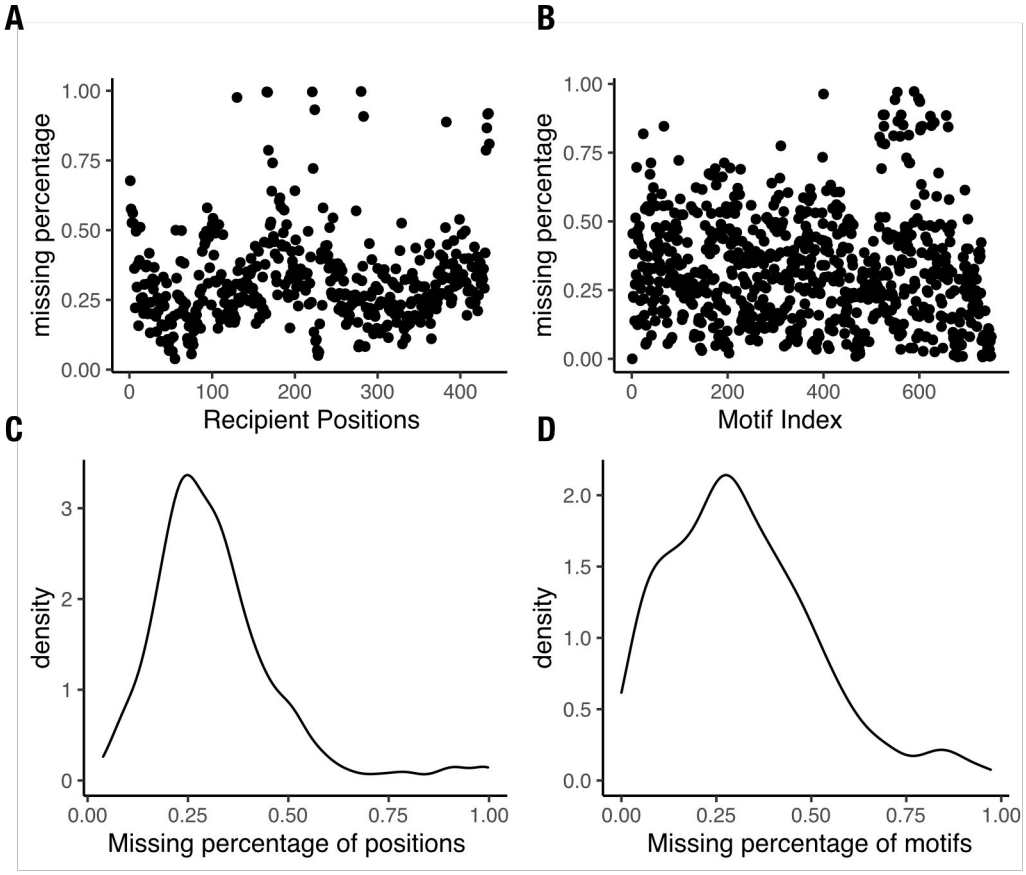


**Supplemental Figure 1: Insertional fitness coverage.** (**A-B**) Scatter plots with the percent missing of Kir2.1 insertion fitness data after alignment by (**A**) position and (**B**) motif. (**C-D**) Density plots of Kir2.1 insertion fitness data percent missing by (**C**) position and (**D**) motif.

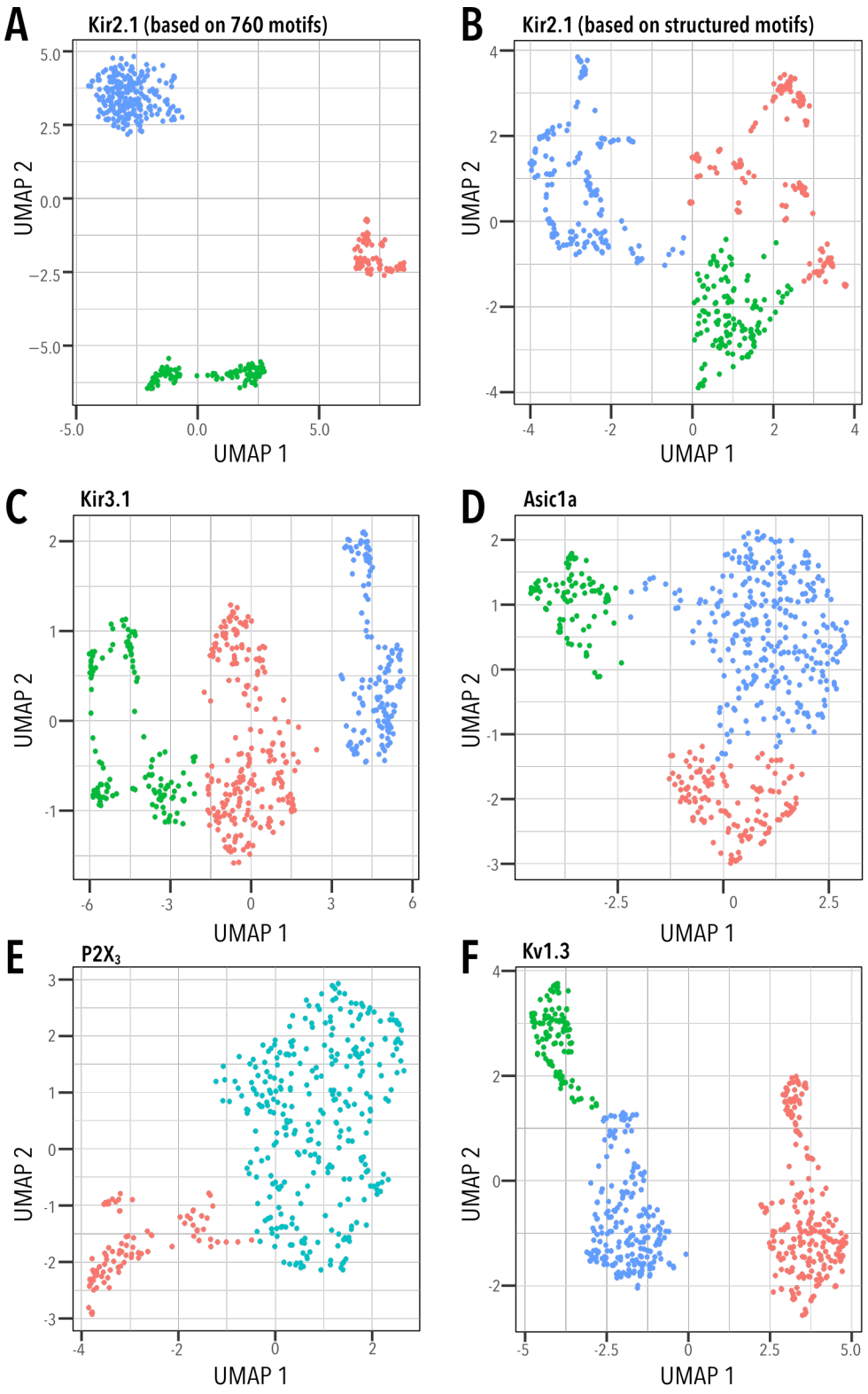


**Supplemental Figure 2: Unbiased clustering of insertion fitness.** Uniform Manifold Approximation Projection (UMAP) was used to cluster insertion fitness of each channel. Cluster membership of each residue is indicated by color. Optimal cluster number was determined using Nbclust (*47*) using the majority rule.

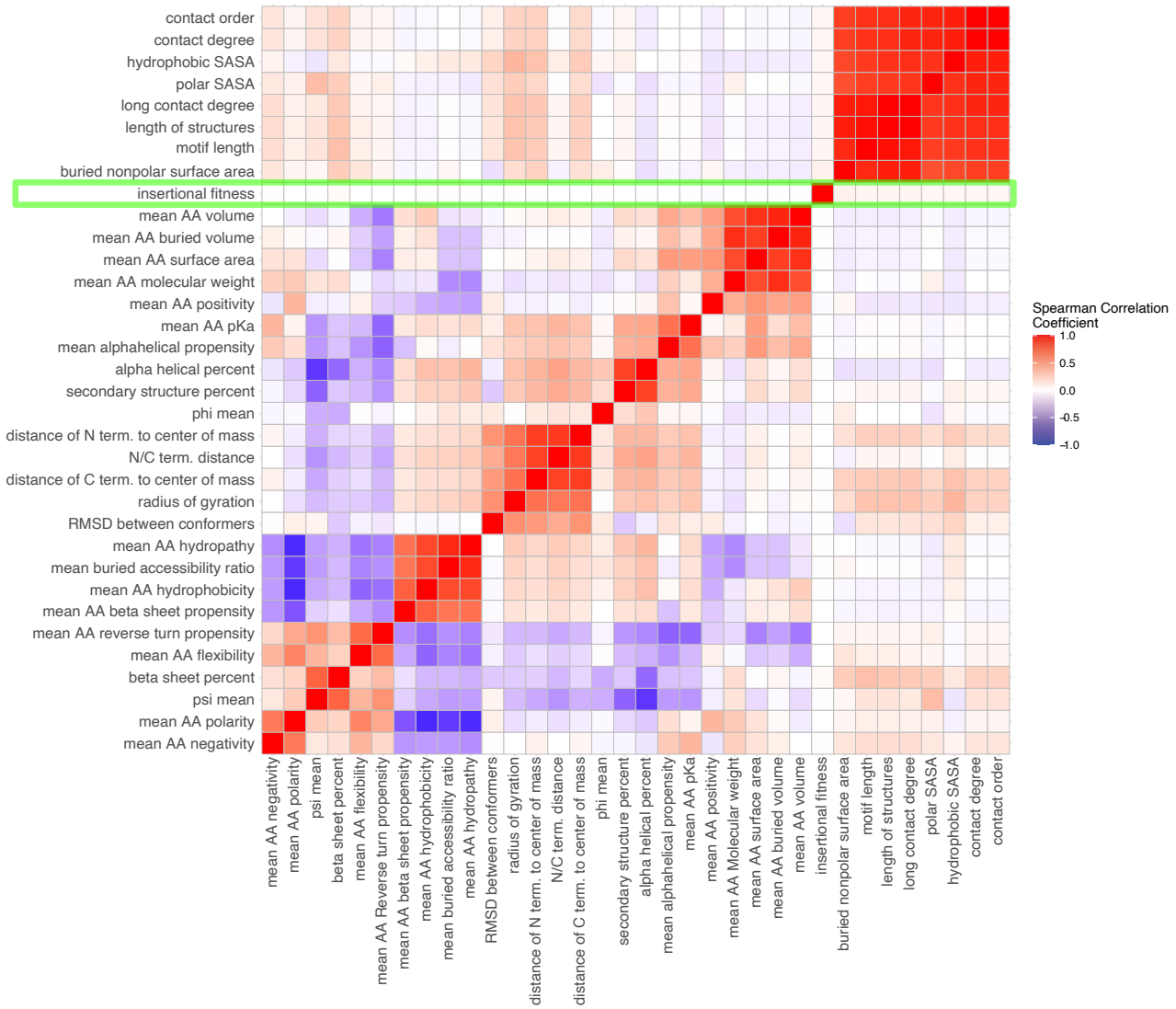


**Supplemental Figure 3: Motif properties and insertional fitness correlations.** Correlation plot between motif property and the fitness across all positions. Insertional fitness is not correlated with any motif property. The motif properties and positions are hierarchically clustered (dendrograms not shown) and the plot is colored with spearman correlations increasing from blue-to-red. AA refers to amino acids and SASA refers to solvent accessible surface area.

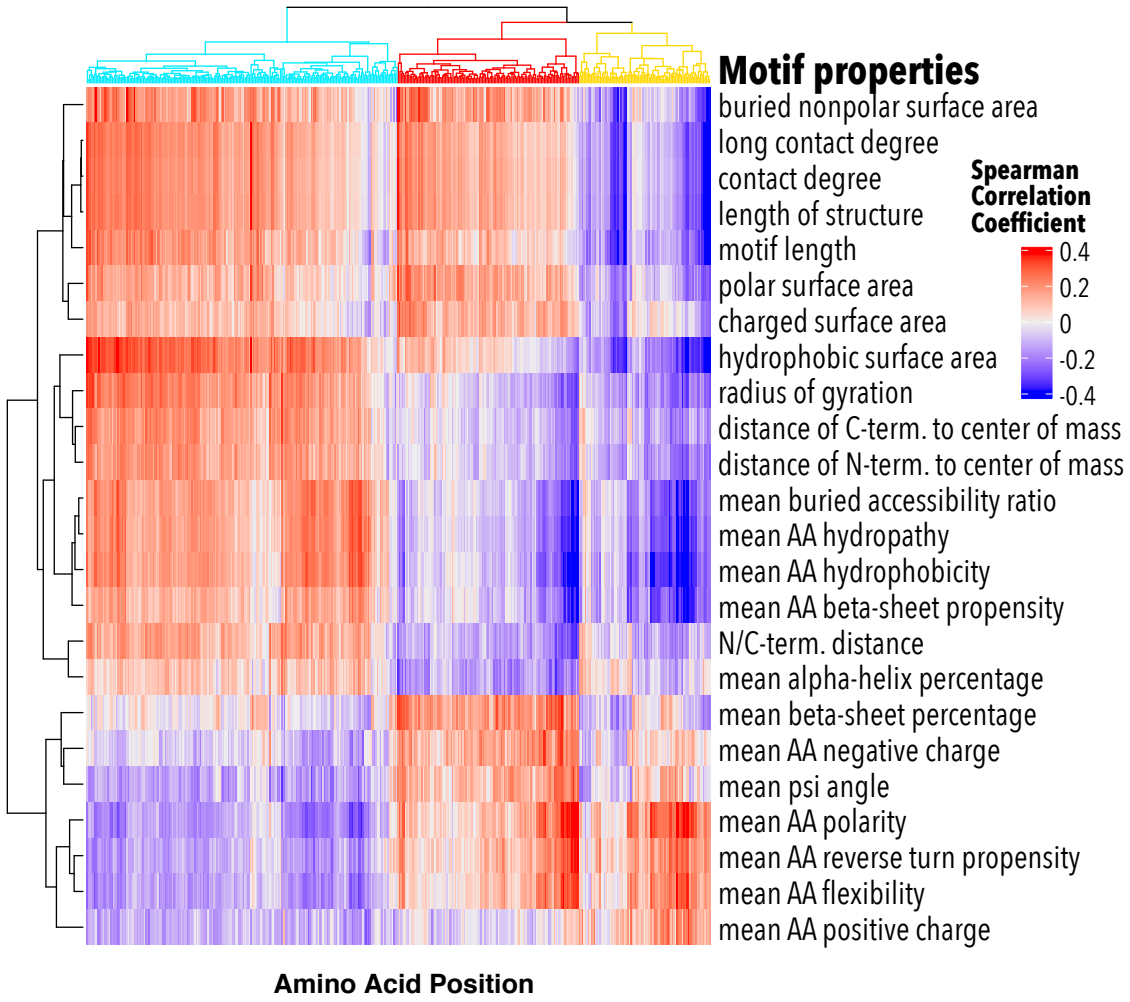


**Supplemental Figure 4: Clustered positions and properties correlation plot.** Correlation plot between motif properties and the fitness of that motif at each position. The motif properties and positions are hierarchically clustered. Position clusters dendogram branches are colored (cyan, red, yellow) as in **Fig. 2L**.

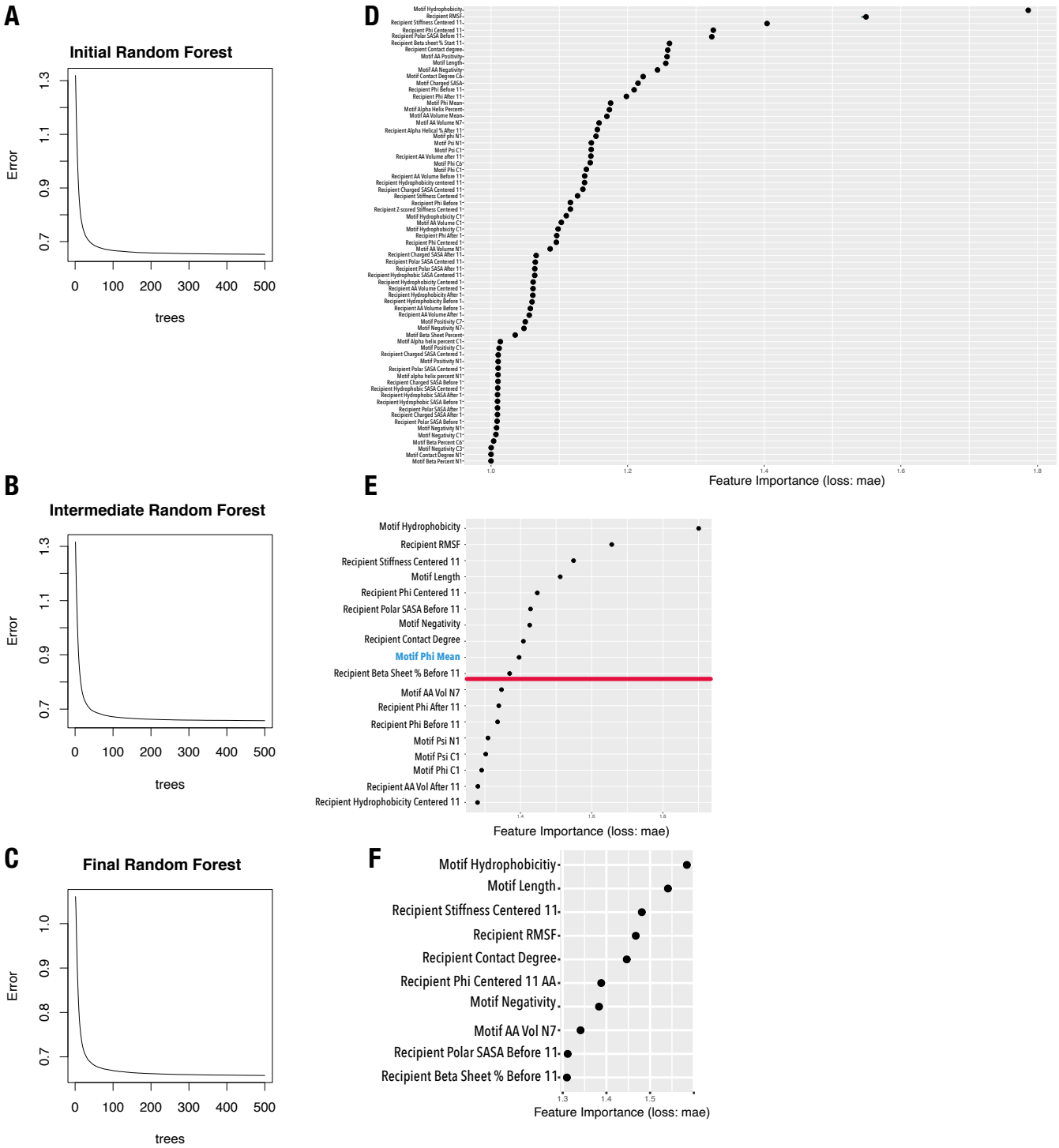


**Supplemental Figure 5: Random Forest model iteration training and property importance.** (**A-C**) Error curves with mean squared error plotted against number of trees in the **(A)** initial, (**B**) intermediate, and (**C**) final Random forest models. As more trees are added there is less error. (**D-F**) Bar plots of the importance of features in predicting insertional fitness in the (**D**) initial, (**E**) intermediate, and (**F**) final Random Forest models. In (**E**) the threshold that was used to trim features is marked with a red line. In addition, mean motif phi angle (blue) was removed because it required motifs to have solved structures, which substantially limited the number of motifs we could include. Property importance is based on the mean absolute error (mae) of removing properties from the predictive model. Further details can be found in the *Materials and Methods*.

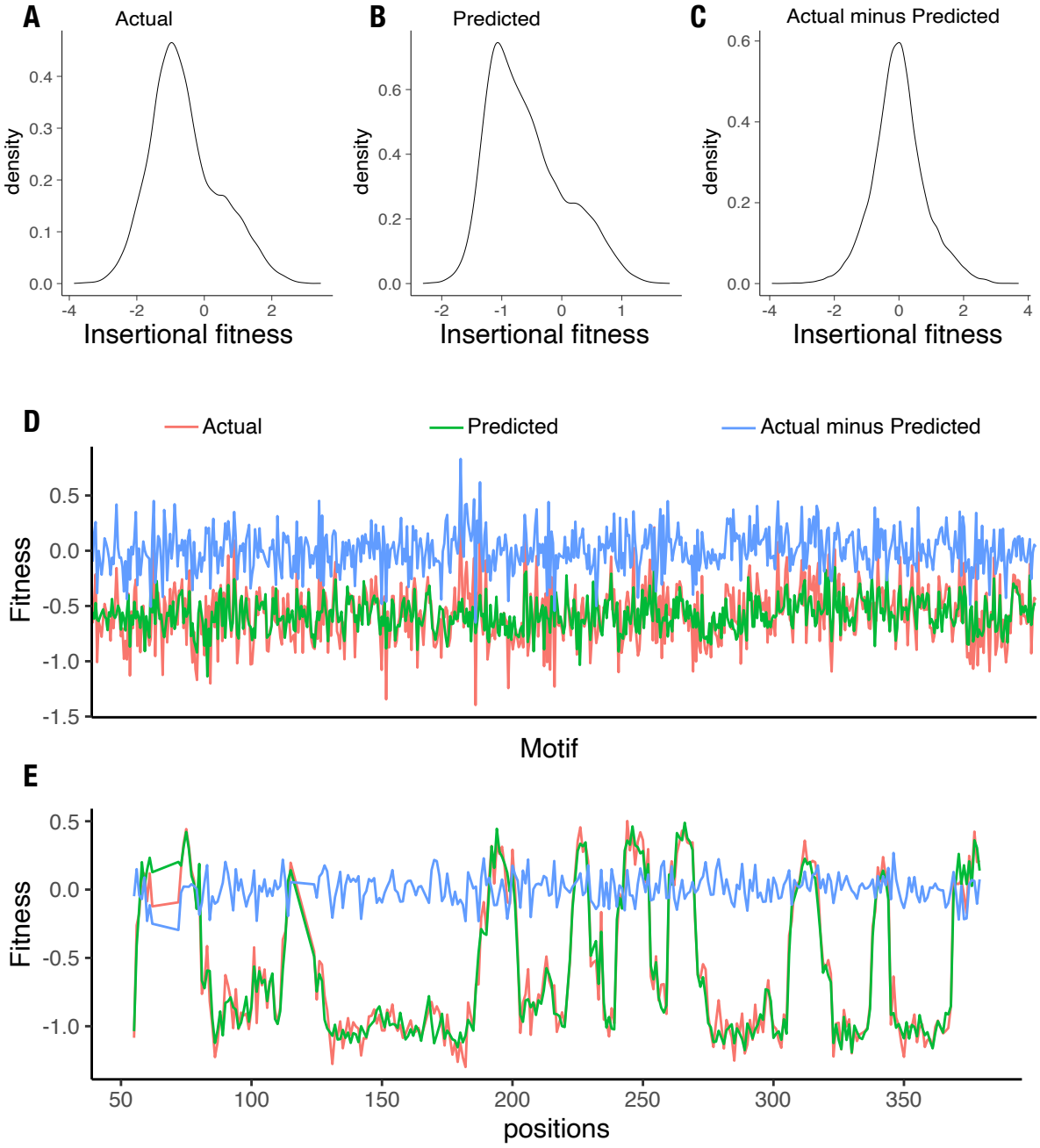


**Supplemental Figure 6: Model performance plots.** (**A-C**) Density plots for (**A**) actual, (**B**) predicted, and (**C**) difference between actual and predicted insertional fitness. (**D**) Insertional fitness actual, predicted, and the difference per domain. (**E**) Insertional fitness actual, predicted, and difference per recipient insertion position. All model performance is reported based on data withheld from all random forest training.

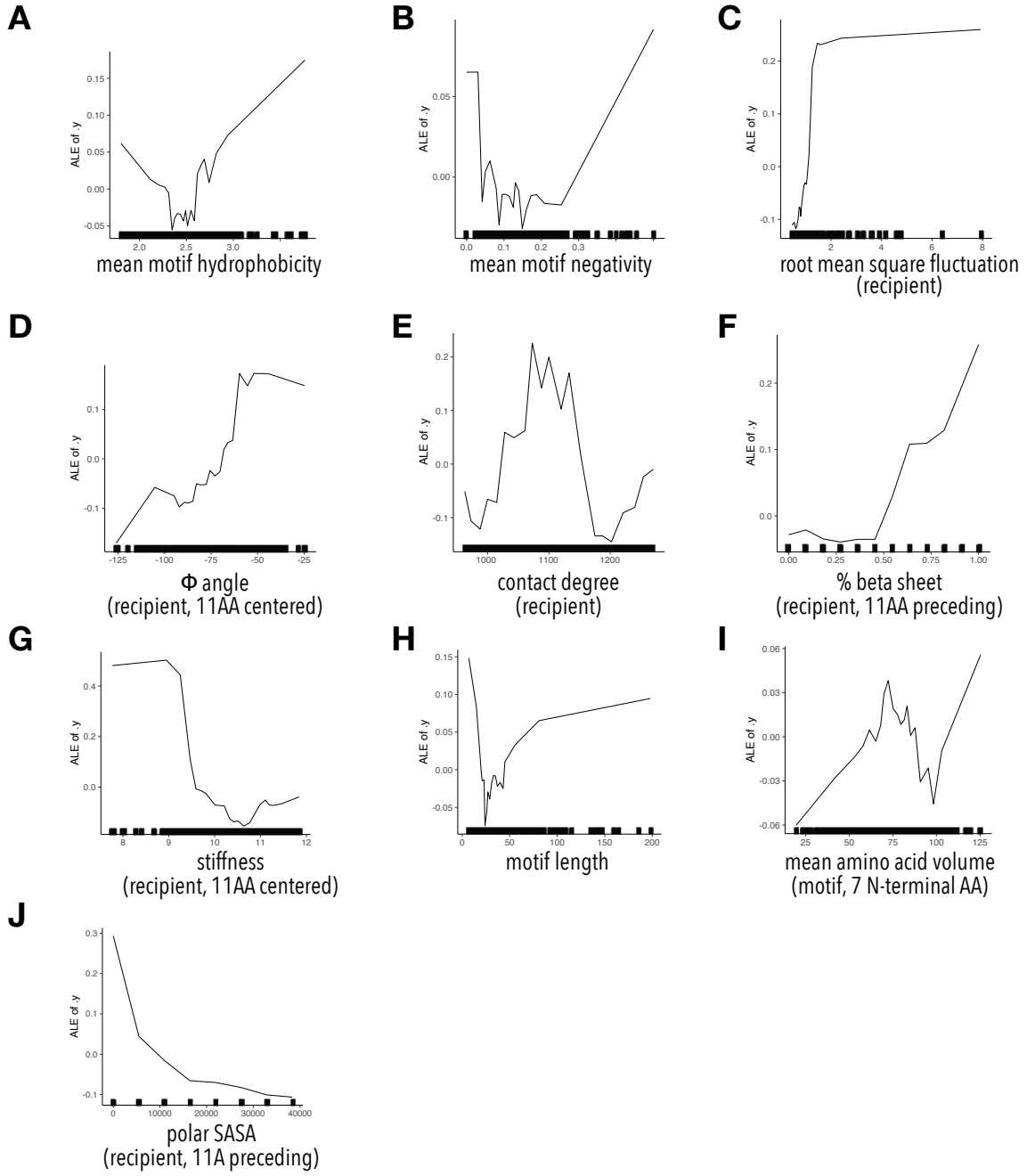


**Supplemental Figure 7: ALE plots for final model properties.** Plots of the Accumulated Local Effects (ALE) of properties on the prediction of insertional fitness for (**A**) mean motif hydrophobicity, (**B)** mean motif negativity, (**C**) recipient root mean square fluctuation (based on MD simulation, PDB code 3JYC), (**D**) mean recipient phi angles of 11 AA centered around insertion site, (**E**) recipient contact density, (**F**) mean beta sheet content 11 AA before insertion site (**G**) mean recipient stiffness of 11 AA centered around insertion site, (**H**) motif length, (**I**) mean amino acid volume of the motif's 7 N terminal AA, and (**J**) polar surface accessible surface area of 11 AA before insertion site.

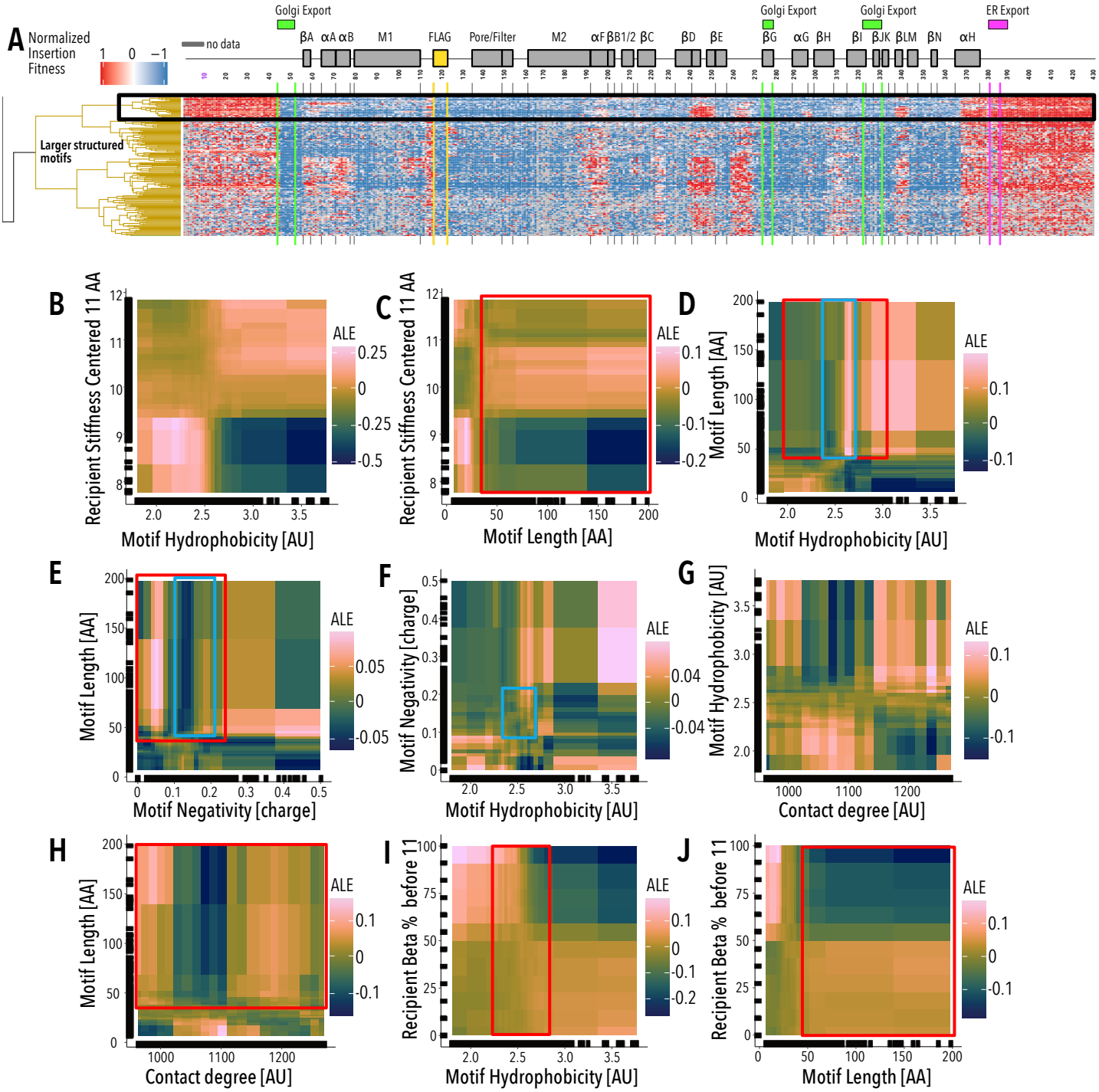


**Supplemental Figure 8: Larger structured motif cluster pairwise ALE Exploration.** (**A**) Insertion fitness heatmap of structured motifs inserted into all positions of Kir2.1. Secondary structural elements (grey boxes) for Kir2.1 are shown above, along known Golgi and ER export signals (green and magenta boxes, respectively). Motifs are hierarchically clustered by on a cosine distance metric. The black box indicates a subset of 'well-structured motifs' (see Fig. 2F-H). (**B-J**) Pairwise ALE plots investigate how pairwise interactions contribute to prediction of (**B**) recipient stiffness - motif hydrophobicity, (**C**) recipient stiffness - motif length, (**D**) motif hydrophobicity - motif length, (**E**) motif length - motif hydrophobicity, (**F**) motif negativity - motif hydrophobicity, (**G**) motif hydrophobicity - recipient contact degree, (**H**) motif length - recipient contact degree, (**I**) recipient Beta % - motif hydrophobicity, and (**J**) recipient beta % - motif length. Pairwise ALE plots are colored from dark blue to pink with increasing ALE scores. The distribution of larger motifs cluster is boxed in red and the distribution of the well-structured is boxed in blue. Marginal ticks (**B–J**) indicate data point used in model building.

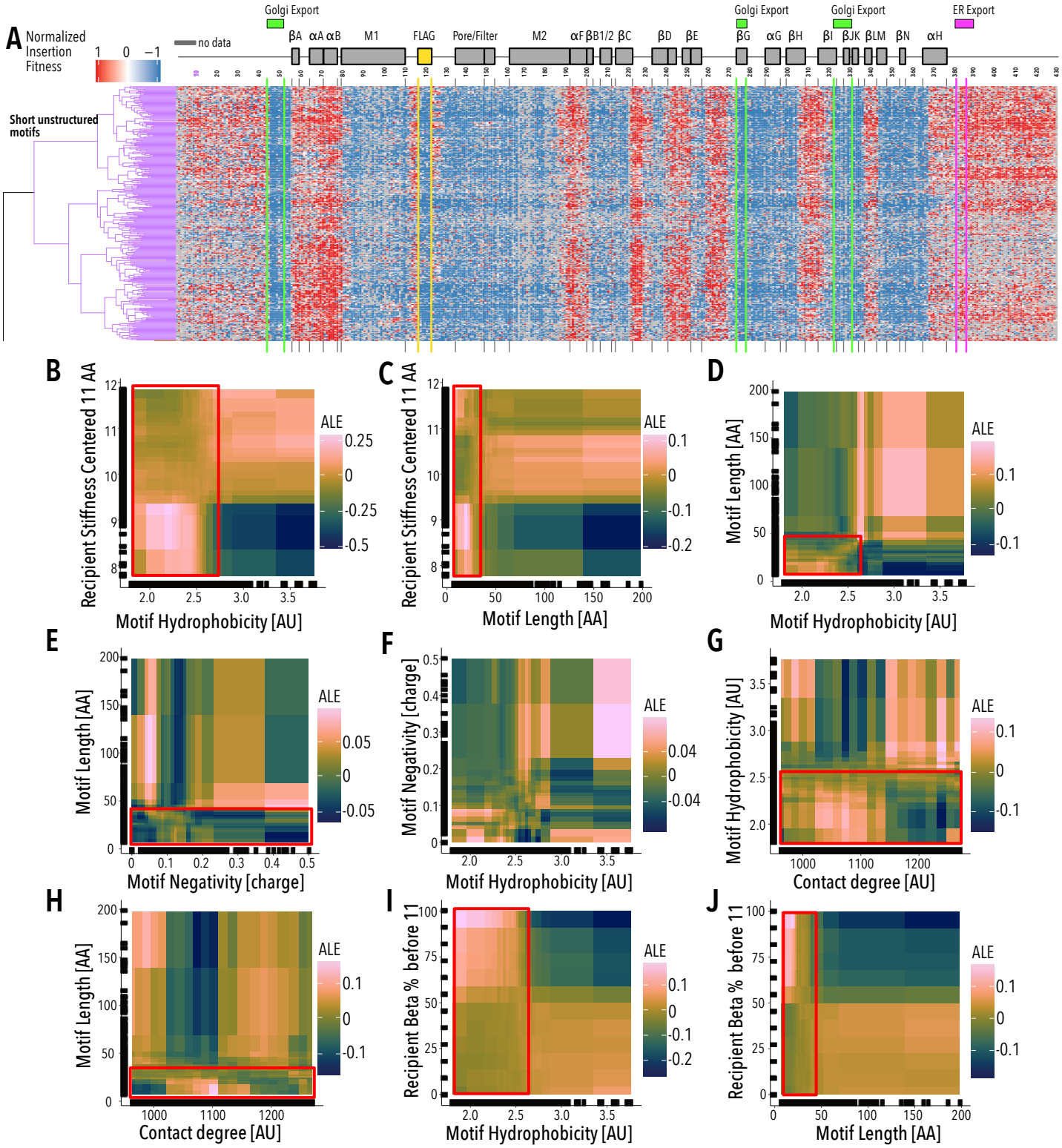


**Supplemental Figure 9: Short unstructured motif cluster pairwise ALE Exploration.** (**A**) Insertion fitness heatmap of short unstructured motifs inserted into all positions of Kir2.1. Secondary structural elements (grey boxes) are Kir2.1 are shown above, along known Golgi and ER export signals (green and magenta boxes, respectively). Motifs are hierarchically clustered by on a cosine distance metric. (**B-J**) Pairwise ALE plots investigate how pairwise interactions contribute to prediction of (**B**) recipient stiffness - motif hydrophobicity, (**C**) recipient stiffness - motif length, (**D**) motif hydrophobicity - motif length, (**E**) motif length - motif hydrophobicity, (**F**) motif negativity - motif hydrophobicity, **(G)** motif hydrophobicity - recipient contact degree, (**H**) motif length - recipient contact degree, (**I**) recipient Beta % - motif hydrophobicity, and (**J**) recipient beta % - motif length. Pairwise ALE plots are colored from dark blue to pink with increasing ALE scores. The distributions of hydrophobic motifs cluster are boxed in red. Marginal ticks (**B–J**) indicate data point used in model building.

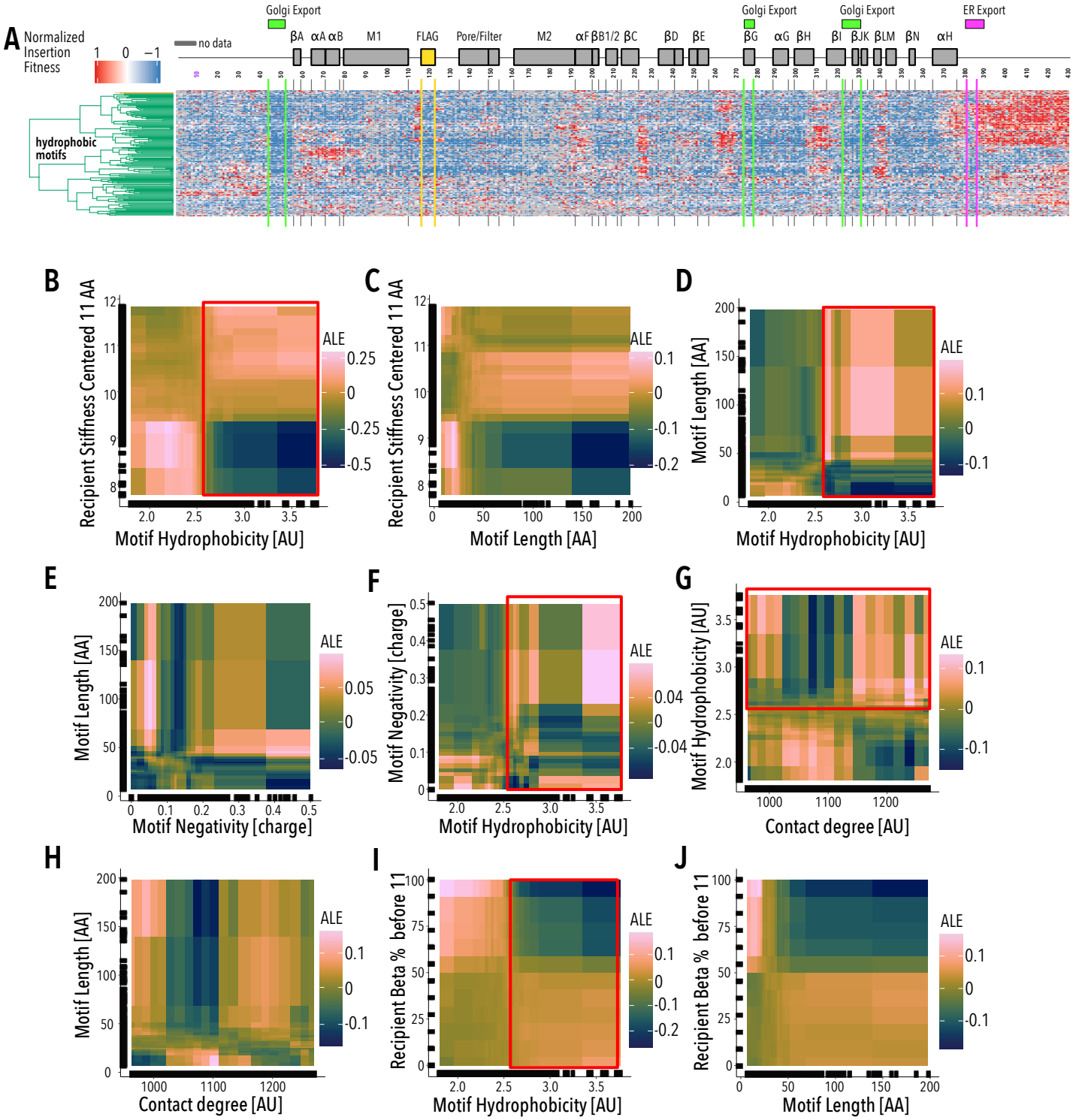


**Supplemental Figure 10: Hydrophobic motif cluster pairwise ALE Exploration.** (**A**) Insertion fitness heatmap of hydrophobic motifs inserted into all positions of Kir2.1. Secondary structural elements (grey boxes) for Kir2.1 are shown above, along known Golgi and ER export signals (green and magenta boxes, respectively). Motifs are hierarchically clustered by on a cosine distance metric. (**B-J**) Pairwise ALE plots investigate how pairwise interactions contribute to prediction of (**B**) recipient stiffness - motif hydrophobicity, (**C**) recipient stiffness - motif length, (**D**) motif hydrophobicity - motif length, (**E**) motif length - motif hydrophobicity, (**F**) motif negativity - motif hydrophobicity, (**G**) motif hydrophobicity - recipient contact degree, **(H)** motif length - recipient contact degree, (**I**) recipient Beta % - motif hydrophobicity, and (**J**) recipient beta % - motif length. Pairwise ALE plots are colored from dark blue to pink with increasing ALE scores. The distributions of hydrophobic motifs cluster are boxed in red. Marginal ticks (**B–J**) indicate data point used in model building.

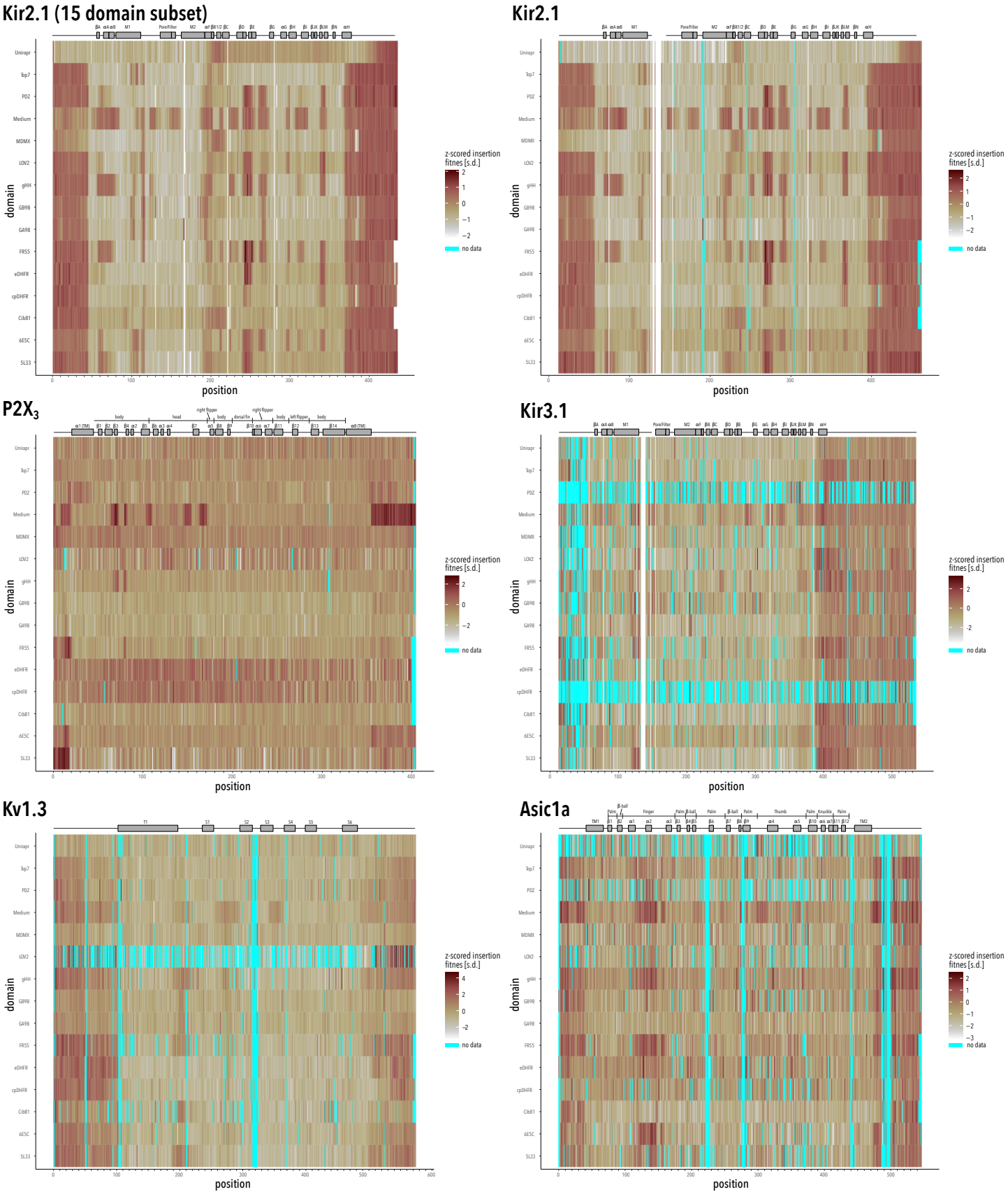


**Supplemental Figure 11: Mean insertion fitness across channels and domains.** All datasets are based on at least two biological replicates. Two datasets are shown for Kir2.1 that were collected with different sequencing chemistry. Secondary structure elements (and topological organization; $P2X_3$ and Asic1a only) are shown as cartoons.

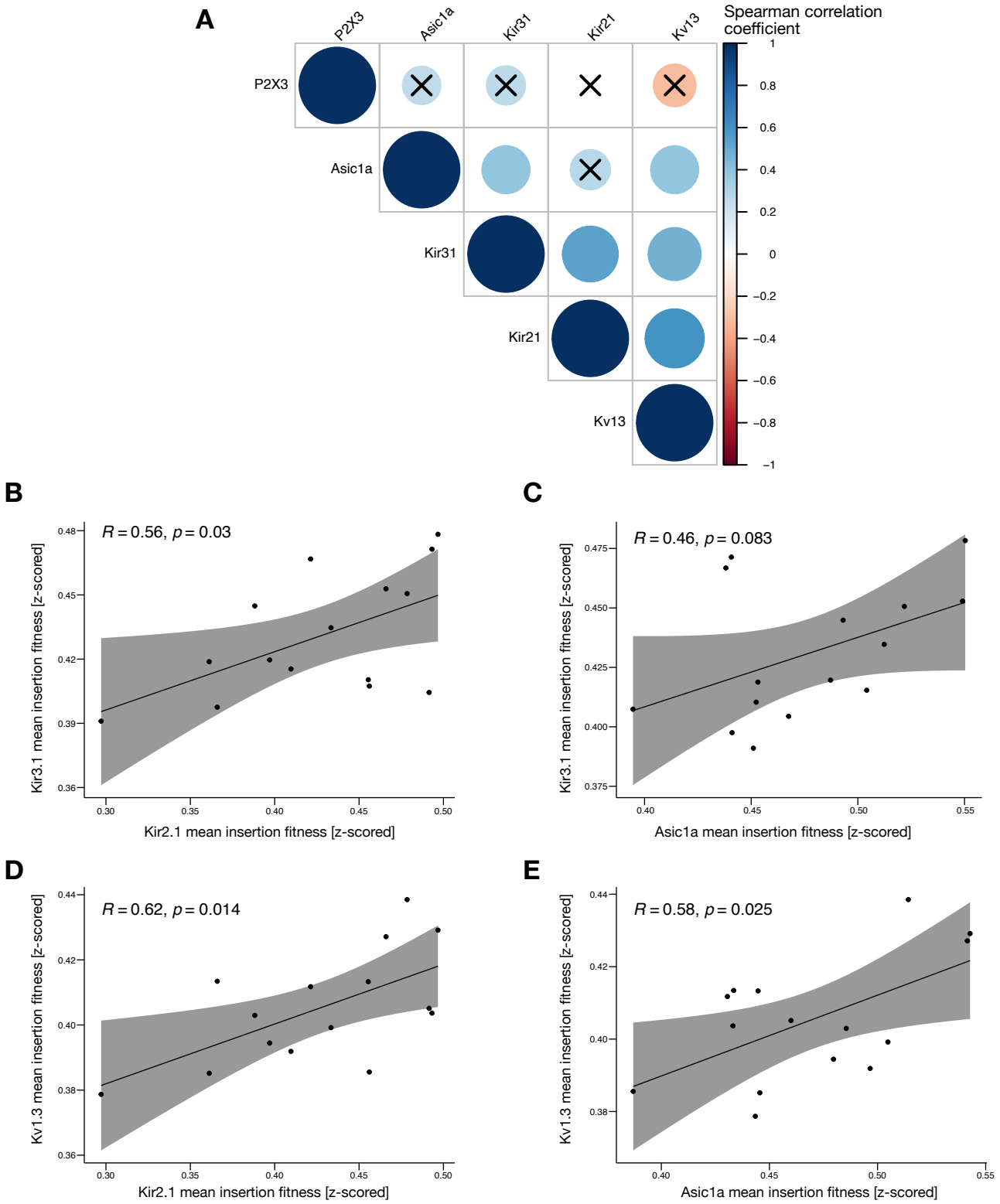


**Supplemental Figure 12: Correlation of domain insertion fitness in different ion channels.** (**A**) Spearman correlation of mean insertion fitness (across all channel positions and motifs) between different channel pairs. Crosses indicate coefficient p-values > 0.05 (i.e., not significant). (**B-E**) Scatterplots of mean insertion fitness (across all channel position) for each inserted motifs. The solid black line indicates a linear regression and the grey shaded area indicates a 90% confidence interval. Spearman correlation coefficient and p-value are shown for each channel combination. Overall, correlation of motif effects on insertion fitness is moderate, suggesting a minor role relative to recipient channel properties.

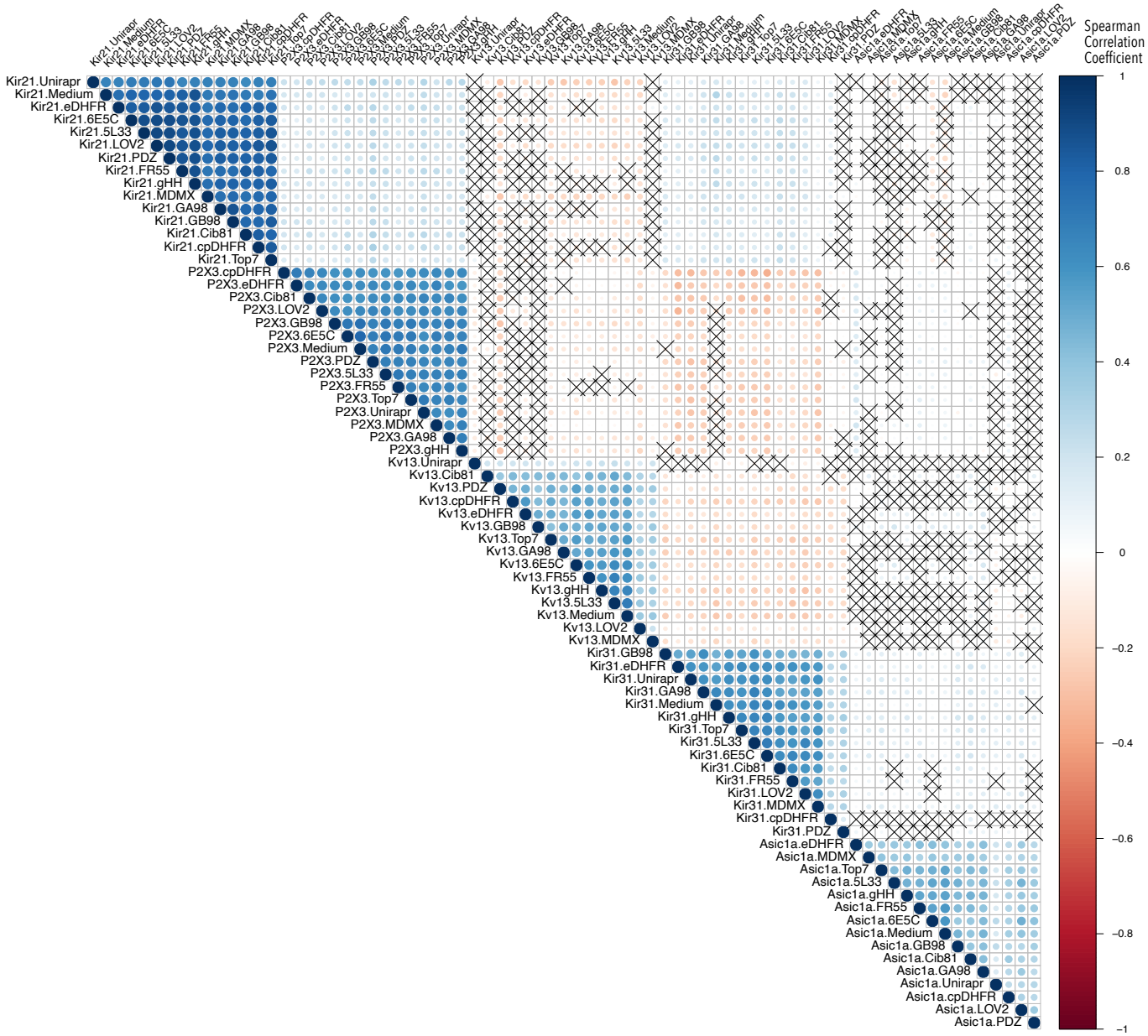


**Supplemental Figure 13: Correlations of insertion fitness for motifs in different channels.** Spearman correlation of mean insertion fitness (across all channel position) of a specific motif in a specific channels with all other combinations. Strong correlations of different motifs in the same channel background dominate, suggesting that the recipient properties' influence on fitness is strong. Crosses indicate coefficient p-values > 0.05 (i.e., not significant).

| class 1 | ligand binding sites N | ligand binding sites Y | |
|---|---|---|---|
| N | 135 | 55 | 190 |
| Y | 195 | 38 | 333 |
| | 330 | 93 | 423 |

p = 0.9994 (n.s.)

| class 2 | ligand binding sites N | ligand binding sites Y | |
|---|---|---|---|
| N | 221 | 93 | 314 |
| Y | 109 | 0 | 109 |
| | 330 | 93 | 423 |

p = 1 (n.s.)

| class 3 | ligand binding sites N | ligand binding sites Y | |
|---|---|---|---|
| N | 304 | 38 | 342 |
| Y | 26 | 55 | 81 |
| | 330 | 93 | 423 |

p = < 2.2e-16 (***)

**Supplemental Figure 14: Class / ligand binding sites contigency tables.** Independence of inward rectifier ligand binding sites ($PIP_2$ – Kir2.1, Kir3.1, Kir6.2, Gβγ – Kir3.1 only, ATP – Kir6.2 only) with respect to different residue classes identified by unbiased clustering of insertion fitness was tested using two-sided Fisher's Exact tests. Only class 3 (colored yellow in **Fig. 1D**) is enriched for ligand binding sites.

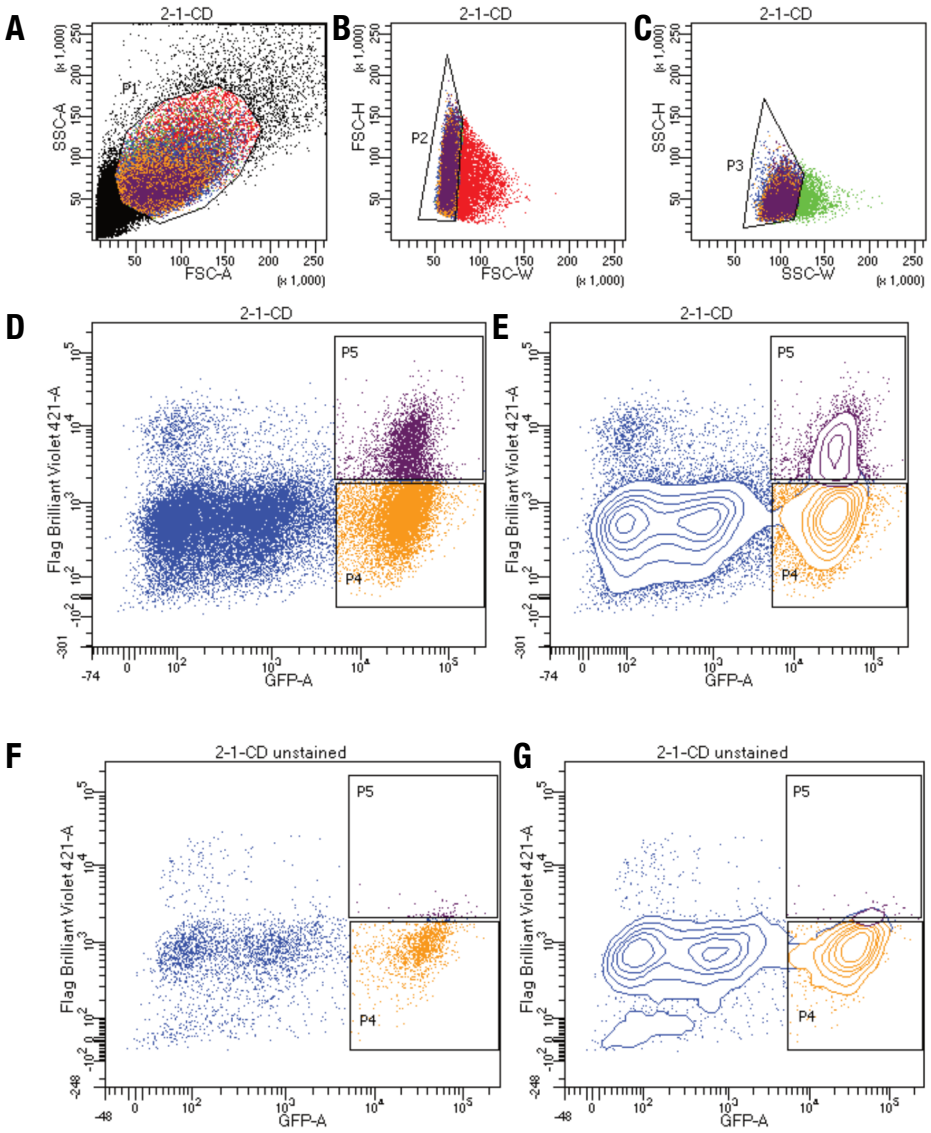


**Supplemental Figure 15: Kir2.1 surface expression assay gating scheme.** (**A**) Whole HEK293 cells are gated on side (SSC-A) and forward scattering (FSC-A). (**B-C**) Forward scattering height (SSC-H), forward scattering width (FSC-W), and Side scattering width (SSC-W) are used to gate single cells. (**D-G**) EGFP$^{high}$/Label$^{low}$ and EGFP$^{high}$/Label$^{high}$ populations are gated based (**D-E**) stained and (**F-G**) unstained on EGFP (GFP-A) of Anti-Flag Brilliant Violet-421 fluorescence with (**D,F**) scatterplot and (**E,G**) contour plots shown. Contour plots represent 95% confidence intervals with outliers shown as dots.

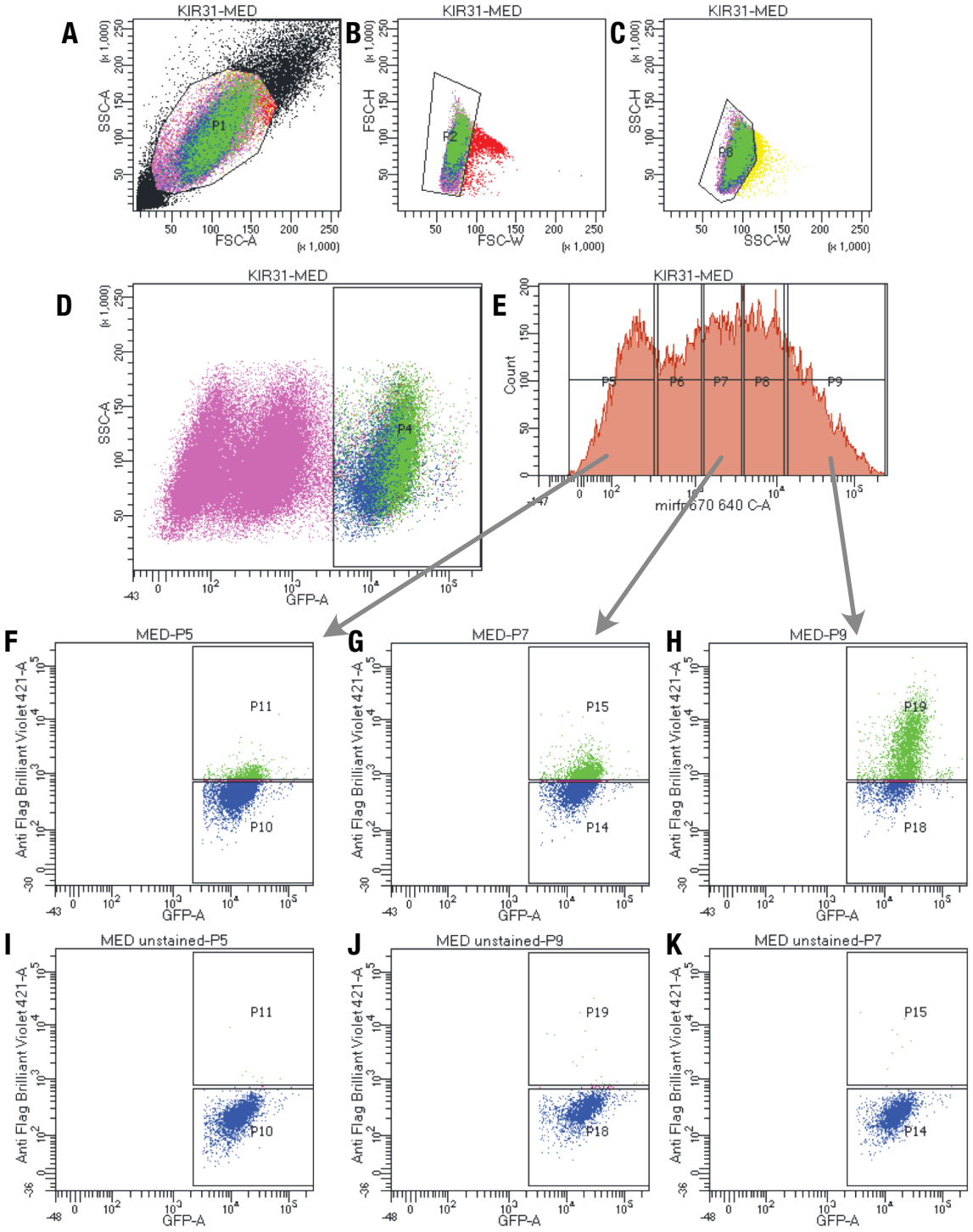


**Supplemental Figure 16: Kir3.1 surface expression assay gating scheme.** (**A**) Whole HEK293 cells are gated on side (SSC-A) and forward scattering (FSC-A). (**B-C**) Forward scattering height (SSC-H), forward scattering width (FSC-W), and Side scattering width (SSC-W) are used to gate single cells. (**D**) Cells are gated on EGFP positive cells to isolate successfully recombined libraries. (**E**) Cells are further split into 5 populations to separate out different populations of Kir3.2 co-expressed miRFP670. (**F-K**) EGFP$^{high}$/ Label$^{low}$ and EGFP$^{high}$/ Label$^{high}$ populations are gated based (**F-H**) stained and (**I-K**) unstained on EGFP (GFP-A) of Anti-Flag Brilliant Violet-421 fluorescence. The data from 3 highest levels of miRFP670 were combined and reported as fitness.

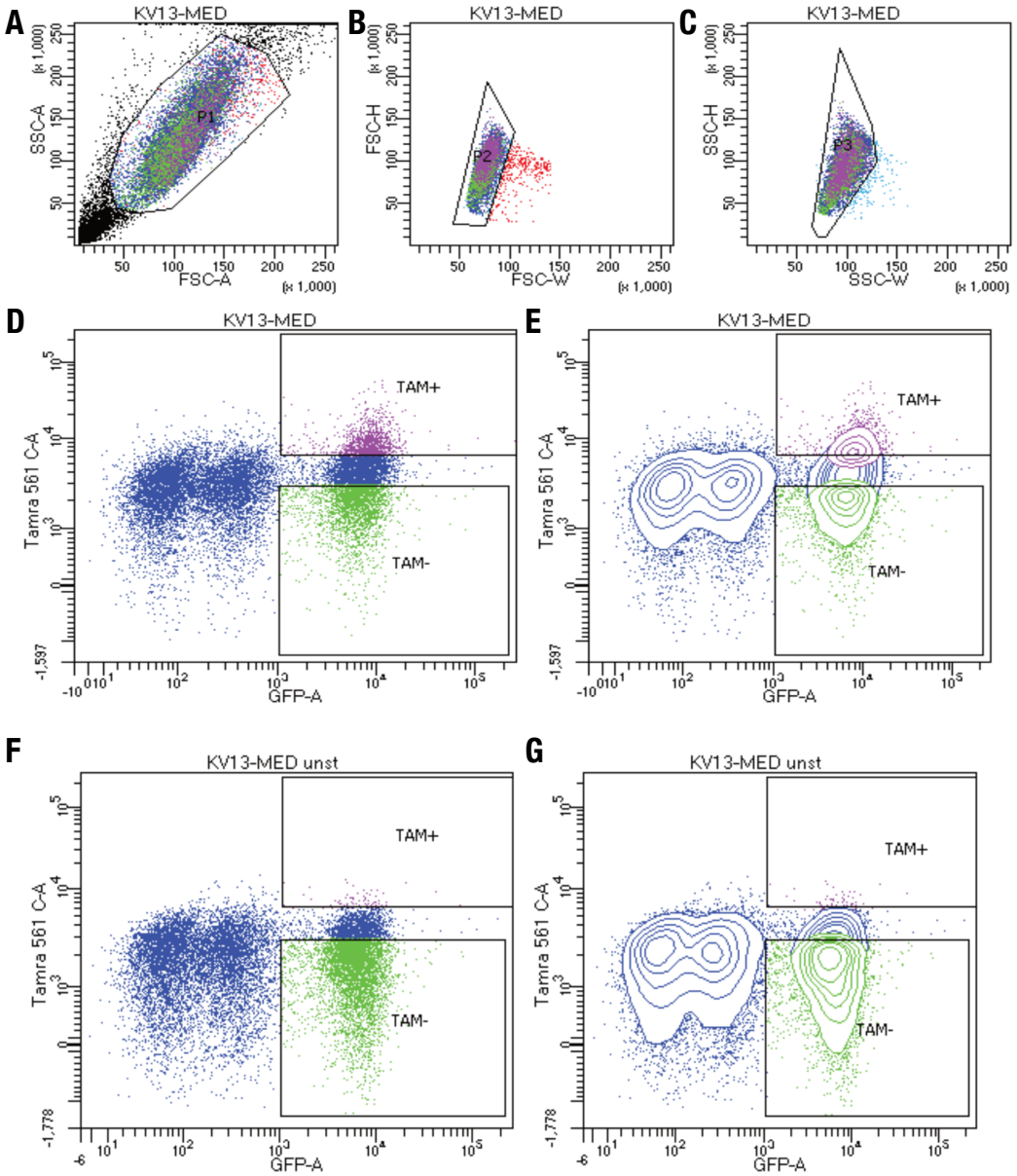


**Supplemental Figure 17: Kv1.3 Surface expression assay gating scheme.** (**A**) Whole HEK293 cells are gated on side (SSC-A) and forward scattering (FSC-A). (**B-C**) Forward scattering height (SSC-H), forward scattering width (FSC-W), and Side scattering width (SSC-W). (**D-G**) EGFP$^{high}$/ Label$^{low}$ and EGFP$^{high}$/Label$^{high}$ populations are gated based (**D-E**) stained and (**F-G**) unstained on EGFP (GFP-A) of Kv1.3 specific Agitoxin-Tamra fluorescence with (**D,F**) scatterplot and (**E,G**) contour plots shown. Contour plots represent 95% confidence intervals with outliers shown as dots.

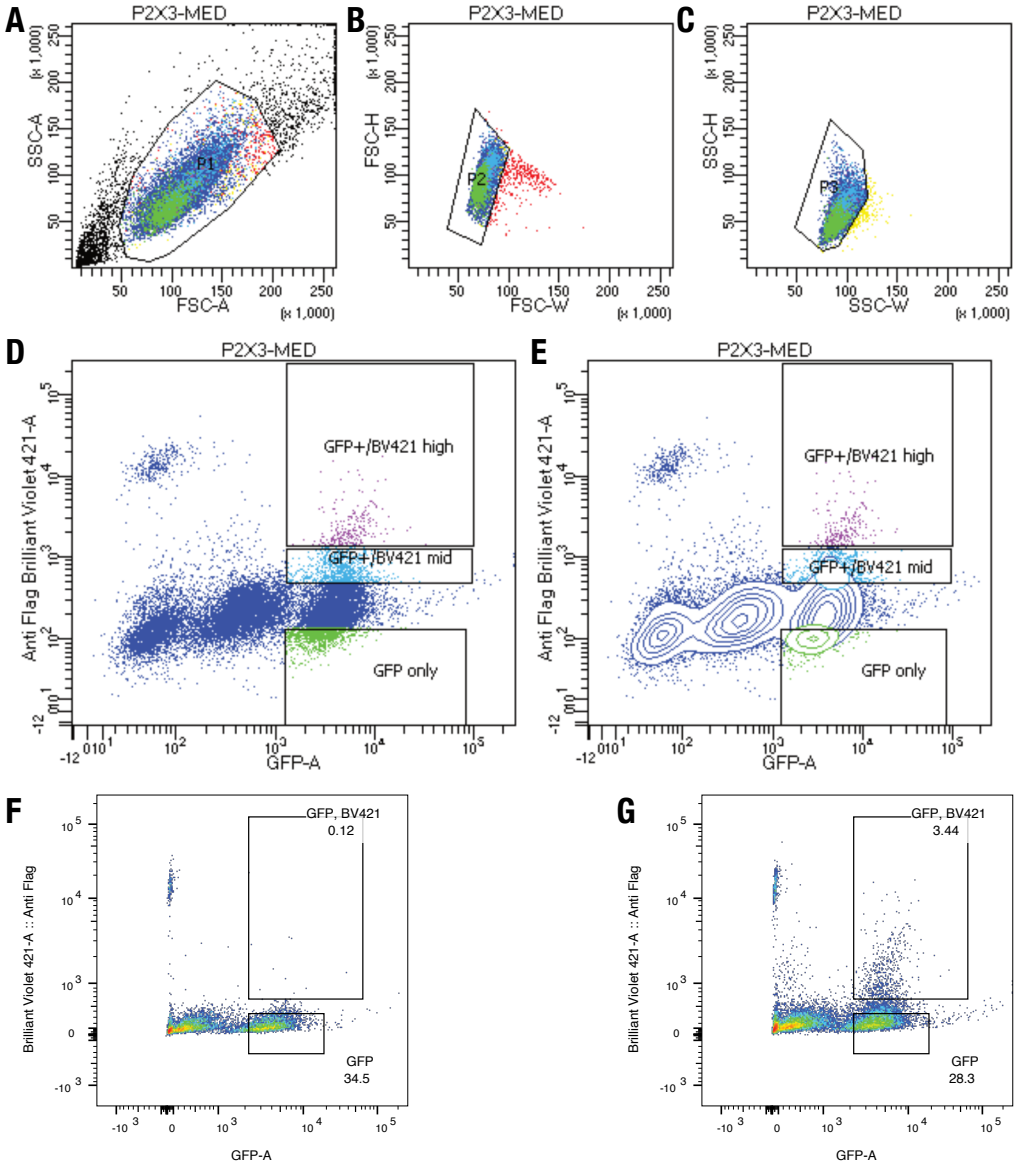


**Supplemental Figure 18: P2X$_3$ Surface expression assay gating scheme.** (**A**) Whole HEK293 cells are gated on side (SSC-A) and forward scattering (FSC-A). (**B-C**) Forward scattering height (SSC-H), forward scattering width (FSC-W), and Side scattering width (SSC-W) are used to gate single cells. (**D-E**) EGFP$^{high}$/ Label$^{low}$, EGFP $^{high}$/Label$^{low}$, EGFP$^{high}$/Label$^{med}$ and EGFP$^{high}$/Label$^{high}$ populations are gated based (**F**) stained and (**G**) unstained on EGFP (GFP-A) of Anti-Flag Brilliant Violet-421 fluorescence with (**D**) scatterplot, (**E**) Contour plot, and (**F-G**) pseudo color plots. In post sample collection *Mid* and *High* label populations were combined ratiometrically based on percent populations in corresponding gates. Contour plots represent 95% confidence intervals with outliers shown as dots. Pseudocolor plots represent density of points with a blue-to-red color scale with increasing density.

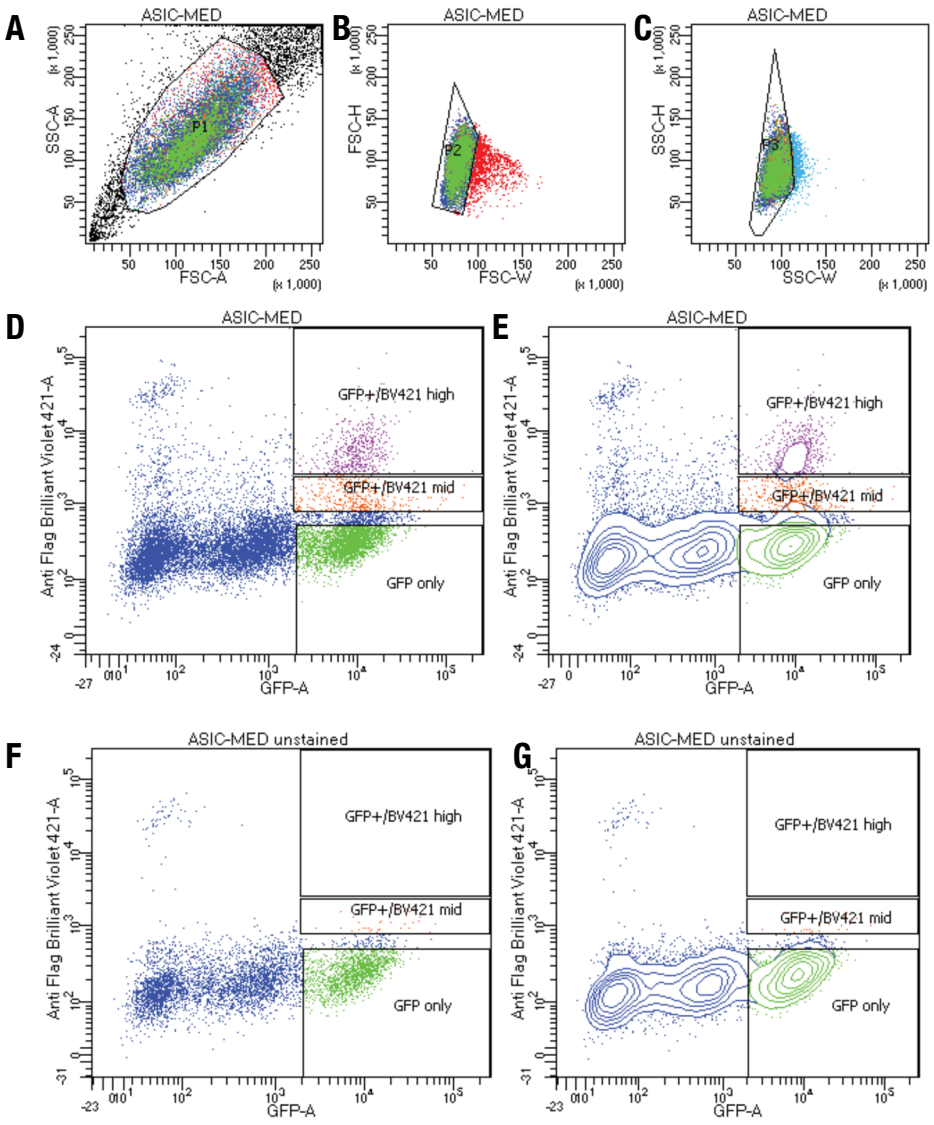


**Supplemental Figure 19: ASIC1a Surface expression assay gating scheme.** (**A**) Whole HEK293 cells are gated on side (SSC-A) and forward scattering (FSC-A). (**B-C**) Forward scattering height (SSC-H), forward scattering width (FSC-W), and Side scattering width (SSC-W) are used to gate single cells. (**D-G**) EGFP$^{high}$/Label$^{low}$ and EGFP$^{high}$/Label$^{high}$ populations are gated based (**D-E**) stained and (**F-G**) unstained on EGFP (GFP-A) of Anti-Flag Brilliant Violet-421 fluorescence with (**D,F**) scatterplot and **(E,G**) contour plots shown. Contour plots represent 95% confidence intervals with outliers as shown as dots.

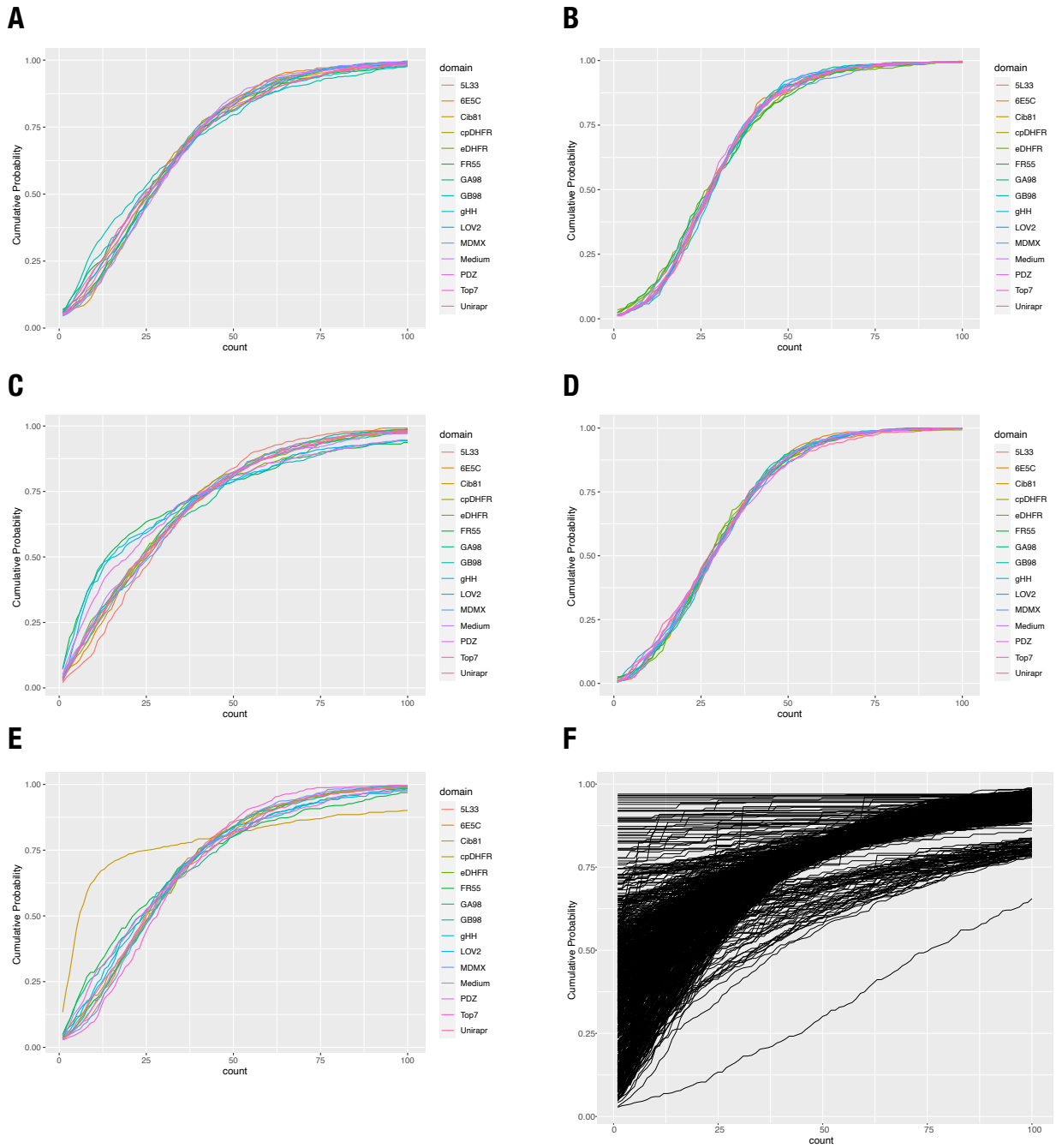


**Supplemental Figure 20: Baseline profiles for each domain and gene combination.** (**A-F)** Empirical cumulative distribution plots for ASIC1a (**A**), Kir2.1 (**B**), Kir3.1 (**C**), P2X3 (**D**), and Kv1.3 (**E**). (**F**) Large domain set for Kir2.1. Each domain was normalized to have 30x coverage before calculating empirical cumulative distribution function. Plots show cumulative probability for each count threshold from 1 to 100. This indicates distribution of insertions in a given gene with distributions shifted to the right being more evenly distributed.

| Motif | Number of motifs | Number of motifs pass QC (%) | Ref. |
|---|---|---|---|
| common domains in extant prot. | 20 | 20 (100%) | (32) |
| disordered protein fragments | 105 | 89 (85%) | (33) |
| disordered proteins | 54 | 27 (50%) | (33) |
| manually curated motifs | 15 | 15 (100%) | n/a |
| polypeptide linkers | 5 | 5 (100%) | n/a |
| ancestral motifs | 40 | 38 (97%) | (34) |
| small non-domain proteins | 6 | 5 (83%) | n/a |
| smotifs | 39 | 38 (97%) | (35) |
| natural proteins < 50 AA | 467 | 391 (84%) | (19) |
| peptide toxins | 9 | 9 (100%) | n/a |
| Total | 760 | 637 (84%) | |

**Supplemental Table 1: Motif group statistics for Kir2.1 760 motif dataset.** Number of motifs, number of motifs passing QC threshold, and sources. Motifs pass QC if they contain statistically significant data in greater than 80% of insertion positions and are included in further analysis and model building.

| Motif property | Abbreviation | Mean +/- SD | Reference |
|---|---|---|---|
| Motif Length [AA] | Motif_length | 37.2 +/- 22.2 | n/a |
| Phi Mean [degrees] | d_phi_mean | -68.0 +/- 12.4 | Pymol |
| Psi Mean [degrees] | d_psi_mean | -0.49 +/- 35.9 | Pymol |
| Radius of Gyration [Å] | d_gyradius | 12.3 +/- 3.3 | Pymol |
| NC distance [Å] | d_nc_dist | 12.3 +/- 3.3 | Pymol |
| Distance of N term to center of mass [Å] | d_center_n_dist | 23.8 +/- 12.8 | Pymol |
| Distance of C term to center of mass [Å] | d_center_c_dist | 23.0 +/- 11.8 | Pymol |
| Contact degree [AU] | d_contact_degree | 450 +/- 287 | (41) |
| Contact order [AU] | d_contact_order | 0.41 +/- 0.038 | (41) |
| Long contact degree [AU] | d_long_degree | 7.99 +/- 9.12 | (41) |
| Secondary Structure (%) | d_sspercent | 60.0 +/- 25.0 | (41) |
| Alpha helical [%] | d_alpha_percent | 53.9 +/- 31.3 | (41) |
| Beta sheet [%] | d_beta_percent | 6.1 +/- 13.6 | (41) |
| Buried nonpolar surface area [$Å^2$] | d_npsa | 2100 +/- 1990 | (41) |
| Charged solvent accessible surface area [$Å^2$] | d_charged_mean | 39,600 +/- 53,700 | (41) |
| Polar solvent accessible surface area [$Å^2$] | d_polar_mean | 40,710 +/- 56,000 | (41) |
| Hydrophobic solvent accessible surface area [$Å^2$] | d_hydrophob_mean | 69,000 +/- 88,000 | (41) |
| Root mean squared deviation between conformers | d_rmsd | 2.98 +/- 2.25 | Pymol |
| Stiffness [AU] | d_stiffness_mean | -7.62E-18 +/- 1.08 E-15 | (40) |
| Mean AA Molecular Weight [Da] | d_AA_MW_mean | 130. +/- 7.49 | (46) |
| Mean AA Surface area [$Å^2$] | d_AA_SA_mean | 158 +/- 16 | (46) |
| Mean AA Alpha helical propensity [AU] | d_AA_alphahel_mean | 1.04 +/- 0.07 | (46) |
| Mean AA Beta sheet propensity [AU] | d_AA_betashe_mean | 0.99 +/- 0.07 | (46) |
| Mean AA Buried accessibility ratio propensity [AU] | d_AA_bur_acc_ratio_mean | 1.25 +/- 0.29 | (46) |
| Mean AA flexibility [AU] | d_AA_flex_mean | 0.44 +/- 0.02 | (46) |
| Mean AA hydropathy [AU] | d_AA_hydropath_mean | -0.43 +/- 0.84 | (46) |
| Mean AA hydrophobicity [AU] | d_AA_hydrophob_mean | 2.5 +/- 0.26 | (46) |
| Mean AA negative charge | d_AA_negat_mean | 0.117 +/- 0.079 | (46) |
| Mean AA pka | d_AA_pka_mean | 4.28 +/- 0.28 | (46) |
| Mean AA polarity [AU] | d_AA_polar_mean | 8.6 +/- 0.7 | (46) |
| Mean AA positive charge | d_AA_posit_mean | 0.17 +/- 0.09 | (46) |
| Mean AA reverse turn propensity [AU] | d_AA_rev_turn_mean | 0.97 +/- 0.11 | (46) |
| Mean AA volume [$Å^3$] | d_AA_vol_mean | 79.1 +/- 10.7 | (46) |
| Length of structures [AA] | d_size | 36.6 +/- 20.1 | (41) |

**Supplemental Table 2:** Inserted motif properties. This table only contains means and standard deviations of the insertion position properties. All additional sliding window recipient properties are provided in a supplemental .csv file. Å refers to Angstroms, AA refers to amino acids, Da refers to Daltons, and AU to arbitrary units.

| Recipient insertion position property | Abbreviation | Mean +/- SD | Reference |
|---|---|---|---|
| MD Root mean square fluctuation 3SPI (AU) | rmsf_3spi | 0.96 +/- 0.70 | n/a |
| MD Root mean square fluctuation 3JYC(AU) | rmsf_3jyc | 1.14 +/- 0.85 | n/a |
| Phi (Degrees) | phi | -75.6 +/- 57.7 | Pymol |
| Psi (Degrees) | psi | 41.3 +/- 88.4 | Pymol |
| Contact degree (AU) | cdegree | 1116.5 +/- 92.0 | (41) |
| Contact order (AU) | corder | 0.439 +/- 0.036 | (41) |
| Long contact degree (AU) | longdegree | 0.863 +/- 0.072 | (41) |
| Secondary Structure (percentage) | ss | 0.60 +/- 0.49 | (41) |
| Alpha helix (percentage) | alpha | 0.33 +/- 47 | (41) |
| Beta sheet (percentage) | beta | 0.27 +/- 0.44 | (41) |
| Buried nonpolar surface area ($A^2$) | npsa | -12.2 +/- 144.4 | (41) |
| Charged solvent accessible surface area ($A^2$) | chargedsasa | 13,069 +/- 24,866 | (41) |
| Polar solvent accessible surface area ($A^2$) | polarsasa | 16,100 +/- 26,697 | (41) |
| Normal Mode based Stiffness (AU) | stiffness | 10.33 +/- 1.12 | (40) |
| AA Surface area ($A^2$) | AA_SA | 159.5 +/- 57.9 | (46) |
| AA Buried accessibility ratio propensity (AU) | AA_bur_acc_ratio | 1.41 +/- 1.17 | (46) |
| AA Alpha helical propensity (AU) | AA_alphahel | 1.03 +/- 0.25 | (46) |
| AA Beta sheet propensity (AU) | AA_betashe | 1.02 +/- 0.26 | (46) |
| AA reverse turn propensity (AU) | AA_rev_turn | 0.94 +/- 0.38 | (46) |
| AA volume ($A^3$) | AA_vol | 79.7 +/- 39.1 | (46) |
| AA flexibility (AU) | AA_flex | 0.438 +/- 0.075 | (46) |
| AA Buried accessibility ratio propensity (AU) | AA_bur_vol | 146 +/- 39 | (46) |
| AA Molecular weight (Da) | AA_MW | 131 +/- 27 | (46) |
| AA positive charge | AA_posit | 0.133 +/- 0.340 | (46) |
| AA negative charge | AA_negat | 0.140 +/- 0.35 | (46) |
| AA pka | AA_pka | 4.33 +/- 1.02 | (46) |
| AA polarity (AU) | AA_polar | 8.43 +/- 2.72 | (46) |
| AA hydropathy (AU) | AA_hydropath | -0.133 +/-3.138 | (46) |
| AA Hydrophobicity (AU) | AA_hydrophob | 2.62 +/- 1.02 | (46) |

**Supplemental Table 3: Recipient insertion position properties.** This table only contains means and standard deviations of the insertion position properties. All additional sliding window recipient properties are provided in a supplemental .csv file. Å refers to Angstroms, AA refers to amino acids, Da refers to daltons, and AU to arbitrary units.

| Random Forest | Variance explained (%) | Mean square residuals | Recipient properties (#) | Motif properties (#) | Total properties (#) |
|---|---|---|---|---|---|
| Initial | 39.89 | 0.652 | 37 | 32 | 69 |
| Intermediate | 39.44 | 0.657 | 10 | 8 | 18 |
| Final | 38.69 | 0.658 | 6 | 4 | 10 |

**Supplemental Table 4: Random forest parameters.** Despite substantially reducing the number of properties, model performance based on variance explained and mean squared residuals are not significantly impacted.

| Motif | Length (AA) | Natural or designed | ref |
|---|---|---|---|
| AGSAGSA | 7 | Designed | n/a |
| Syntrophin PDZ | 86 | Natural | (48) |
| Cib81 | 81 | Natural | (49) |
| e. coli cpDHFR | 164 | Modified | (50) |
| e. coli DHFR | 164 | Natural | (51) |
| FR55 | 82 | Designed | n/a |
| GA98 | 56 | Designed | (52) |
| GB98 | 56 | Designed | (52) |
| ghhh06 | 43 | Designed | (53) |
| Unirapr | 198 | Designed | (54) |
| asLOV2 | 143 | Natural | (55) |
| MDMX | 103 | Natural | (56) |
| Top7 | 99 | Designed | (57) |
| 5L33 | 108 | Designed | (58) |
| 6E5C | 73 | Designed | (59) |

**Supplemental table 5: Smaller set of 15 motifs.**

| Pool Name | Gene | Sample | Replicate | Total Reads in Pool | Mean Quality | Aligned Reads | Number of Domains | Number of Positions | Number of Variants | Coverage [x-fold] |
|---|---|---|---|---|---|---|---|---|---|---|
| base_1-16 | Kir2.1 | Baseline | 1 | 81,371,890 | 30.85 | 7482860 | 560 | 436 | 244160 | 30.6 |
| base_17-21 | Kir2.1 | Baseline | 1 | 24,346,753 | 30.92 | 2097244 | 175 | 436 | 76300 | 27.5 |
| base_CD | Kir2.1 | Baseline | 1 | 4,304,294 | 31.17 | 341611 | 45 | 436 | 19620 | 17.4 |
| dp_1_1-16 | Kir2.1 | Surface expression | 1 | 79,873,354 | 30.93 | 7767341 | 560 | 436 | 244160 | 31.8 |
| dp_1_17-21 | Kir2.1 | Surface expression | 1 | 19,242,372 | 30.73 | 1511063 | 175 | 436 | 76300 | 19.8 |
| dp_1_CD | Kir2.1 | Surface expression | 1 | 2,847,220 | 29.28 | 124711 | 45 | 436 | 19620 | 6.4 |
| dp_2_11-12X15 | Kir2.1 | Surface expression | 2 | 9,683,945 | 30.45 | 764060 | 105 | 436 | 45780 | 16.7 |
| dp_2_13-14X18 | Kir2.1 | Surface expression | 2 | 10,853,687 | 31.1 | 311539 | 105 | 436 | 45780 | 6.8 |
| dp_2_19-21X16-17 | Kir2.1 | Surface expression | 2 | 19,264,855 | 29.38 | 1289393 | 175 | 436 | 76300 | 16.9 |
| dp_2_3-10 | Kir2.1 | Surface expression | 2 | 35,490,287 | 30.73 | 2762399 | 280 | 436 | 122080 | 22.6 |
| dp_2_CD | Kir2.1 | Surface expression | 2 | 3,203,291 | 31.36 | 211588 | 45 | 436 | 19620 | 10.8 |
| gfp_1_1-16 | Kir2.1 | No surface expression | 1 | 77,668,001 | 30.82 | 7768024 | 560 | 436 | 244160 | 31.8 |
| gfp_1_17-21 | Kir2.1 | No surface expression | 1 | 27,686,561 | 30.69 | 2270580 | 175 | 436 | 76300 | 29.8 |
| gfp_1_CD | Kir2.1 | No surface expression | 1 | 4,408,355 | 31.78 | 382483 | 45 | 436 | 19620 | 19.5 |
| gfp_2_11-12X15 | Kir2.1 | No surface expression | 2 | 9,433,539 | 31.35 | 937905 | 105 | 436 | 45780 | 20.5 |
| gfp_2_13-14X18 | Kir2.1 | No surface expression | 2 | 9,369,676 | 31.12 | 306212 | 105 | 436 | 45780 | 6.7 |
| gfp_2_19-21X16-17 | Kir2.1 | No surface expression | 2 | 21,731,747 | 30.28 | 2014803 | 175 | 436 | 76300 | 26.4 |
| gfp_2_3-10 | Kir2.1 | No surface expression | 2 | 37,722,582 | 30.96 | 3698554 | 280 | 436 | 122080 | 30.3 |
| gfp_2_CD | Kir2.1 | No surface expression | 2 | 5,126,808 | 30.53 | 415326 | 45 | 436 | 19620 | 21.2 |
| | Asic1a | High surface expression | 1 | | | 330452 | 15 | 546 | 8190 | 40.3 |
| | Asic1a | Low surface expression | 1 | | | 477966 | 15 | 546 | 8190 | 58.4 |
| | Asic1a | No surface expression | 1 | | | 661693 | 15 | 546 | 8190 | 80.8 |
| | Asic1a | High surface expression | 2 | | | 661693 | 15 | 546 | 8190 | 80.8 |
| | Asic1a | Low surface expression | 2 | | | 477966 | 15 | 546 | 8190 | 58.4 |
| | Asic1a | No surface expression | 2 | | | 330452 | 15 | 546 | 8190 | 40.3 |
| | P2X4 | High surface expression | 1 | | | 242095 | 15 | 396 | 5940 | 40.8 |
| | P2X4 | Low surface expression | 1 | | | 609143 | 15 | 396 | 5940 | 102.5 |
| | P2X4 | No surface expression | 1 | | | 464622 | 15 | 396 | 5940 | 78.2 |
| | P2X4 | High surface expression | 2 | | | 328645 | 15 | 396 | 5940 | 55.3 |
| | P2X4 | Low surface expression | 2 | | | 399762 | 15 | 396 | 5940 | 67.3 |
| | P2X4 | No surface expression | 2 | | | 687217 | 15 | 396 | 5940 | 115.7 |
| | P2X3 | High surface expression | 1 | | | 249510 | 15 | 405 | 6075 | 41.1 |
| | P2X3 | Low surface expression | 1 | | | 580254 | 15 | 405 | 6075 | 95.5 |
| | P2X3 | No surface expression | 1 | | | 881800 | 15 | 405 | 6075 | 145.2 |
| | P2X3 | High surface expression | 2 | | | 379725 | 15 | 405 | 6075 | 62.5 |
| | P2X3 | Low surface expression | 2 | | | 489186 | 15 | 405 | 6075 | 80.5 |
| | P2X3 | No surface expression | 2 | | | 918149 | 15 | 405 | 6075 | 151.1 |
| | Asic2a | High surface expression | 1 | | | 455576 | 15 | 520 | 7800 | 58.4 |
| | Asic2a | Low surface expression | 1 | | | 688644 | 15 | 520 | 7800 | 88.3 |
| | Asic2a | No surface expression | 1 | | | 848345 | 15 | 520 | 7800 | 108.8 |
| | Kv1.3 | Surface expression | 1 | | | 434511 | 15 | 575 | 8625 | 50.4 |
| | Kv1.3 | No surface expression | 1 | | | 744064 | 15 | 575 | 8625 | 86.3 |
| | Kv1.3 | Surface expression | 2 | | | 798555 | 15 | 575 | 8625 | 92.6 |
| | Kv1.3 | No surface expression | 2 | | | 810399 | 15 | 575 | 8625 | 94.0 |
| | Kir3.2 | Surface expression | 1 | | | 829744 | 15 | 425 | 6375 | 130.2 |
| | Kir3.2 | No surface expression | 1 | | | 766766 | 15 | 425 | 6375 | 120.3 |
| | Kir3.2 | Surface expression | 2 | | | 988708 | 15 | 425 | 6375 | 155.1 |
| | Kir3.2 | No surface expression | 2 | | | 1025554 | 15 | 425 | 6375 | 160.9 |
| | Kir2.1 | High surface expression | 1 | | | 324519 | 15 | 436 | 6540 | 49.6 |
| | Kir2.1 | Low surface expression | 1 | | | 657683 | 15 | 436 | 6540 | 100.6 |
| | Kir2.1 | No surface expression | 1 | | | 771084 | 15 | 436 | 6540 | 117.9 |
| | Kir2.1 | High surface expression | 2 | | | 613817 | 15 | 436 | 6540 | 93.9 |
| | Kir2.1 | Low surface expression | 2 | | | 521489 | 15 | 436 | 6540 | 79.7 |
| | Kir2.1 | No surface expression | 2 | | | 1110887 | 15 | 436 | 6540 | 169.9 |
| | Kir6.2 | Surface expression | 1 | | | 1230567 | 15 | 410 | 6150 | 200.1 |
| | Kir6.2 | No surface expression | 1 | | | 1377532 | 15 | 410 | 6150 | 224.0 |
| | Kir6.2 | Surface expression | 2 | | | 710829 | 15 | 410 | 6150 | 115.6 |
| | Kir6.2 | No surface expression | 2 | | | 1066743 | 15 | 410 | 6150 | 173.5 |
| | Kir3.1 | No surface expression | 1 | | | 1007295 | 15 | 509 | 7635 | 131.9 |
| | Kir3.1 | Surface expression | 1 | | | 770673 | 15 | 509 | 7635 | 100.9 |
| | Kir3.1 | No surface expression | 2 | | | 764153 | 15 | 509 | 7635 | 100.1 |
| | Kir3.1 | Surface expression | 2 | | | 801705 | 15 | 509 | 7635 | 105.0 |

**Supplemental Table 6: Read count statistics.**